Human finger subjected to shock vibration loading

Master's thesis in Applied Mechanics

Johan Nilsson and David Oljelund

DEPARTMENT OF MECHANICS AND MARITIME SCIENCES

CHALMERS UNIVERSITY OF TECHNOLOGY
Gothenburg, Sweden 2022
www.chalmers.se

MASTER'S THESIS 2022

Human finger subjected to shock vibration loading

Johan Nilsson & David Oljelund

Department of Mechanics and Maritime Sciences
Division of Dynamics
CHALMERS UNIVERSITY OF TECHNOLOGY
Gothenburg, Sweden 2022

Human finger subjected to shock vibration loading

Supervisor: Hans Lindell, Komponenttillverkning, RISE.
Supervisor: Dr. Petri Piiroinen, Division of Dynamics.
Examiner: Prof. Håkan Johansson, Division of Dynamics.

Master's Thesis 2022:50
Department of Mechanics and Maritime Sciences
Division of Dynamics
Chalmers University of Technology
SE-412 96 Gothenburg
Telephone +46 31 772 1000

Typeset in LaTeX
Printed by Chalmers Reproservice
Gothenburg, Sweden 2022

Human finger subjected to shock vibration loading
JOHAN NILSSON
DAVID OLJELUND
Department of Mechanics and Maritime Sciences
Division of Dynamics
Chalmers University of Technology

Abstract

In Sweden it is estimated that around 330 000 workers use vibrating hand-held tools with an exposure of at least 2 hours per day. The damage of hand transmitted vibrations for hand-held tools within the frequency span 6.3 - 1250 Hz have been studied and are described by the international standard ISO 5349. The potential damage of exposure to higher frequencies is however not currently described by the standard and the human response of exposure is not known. Previous work has studied a 2D Finite Element model representing a human finger to investigate effects of shock waves, i.e. waves with high-frequency (above 1250 Hz) transients. However, those attempts were made without access to experimental data, and without clear distinction between the effects from geometry, material properties and FE-mesh. Therefore a 1D FE model of a finger was developed to study these effects on propagating waves. For comparison with experiment output, the 1D FE model was tested with a real input load.

The experiments made on real fingers examined the effects from different fingers, loading magnitude, dates. In addition, acetone and electro-conductive gel was applied to the fingers to study the consistency of the finger response as well as the influence of fingerprints. Furthermore, two types of substitute fingers, ballistic gel and silicon, with different materials substituting bone were produced and tested to see if an increased consistency of the response could be achieved. This was concluded into recommendations for future implementations for the 2D FE model.

It was concluded that the dynamic response and wave propagation velocity did not change significantly without the fingerprint. The substitute fingers tested did not behave more consistently than the real fingers. For the 1D FE model it was concluded that in order to capture the experimental output better it is needed to study the damping of the finger to better model the damping. Additionally, the bone in the finger significantly affect the reflection and transmission of the wave.

Keywords: LS DYNA, experiment, vibration, human finger, ISO 5349, FE model.

Preface

This master thesis is a collaborative project between the Division of Dynamics at Chalmers University of Technology and Research Institutes of Sweden (RISE). The thesis was conducted as a 30 credits project as part of the applied mechanics masters program during spring of 2022.

Acknowledgements

We would like to thank supervisors Petri Piiroinen, Hans Lindell and examiner Håkan Johansson for great support and guidence through the duration of the thesis work. Special thanks to Peter Ottosson at RISE for showing great patience, kindness and support. Big thanks to Marcus Lilja and David Aspenberg at DYNAMORE Nordic. Finally we would like to thank Johan Ireaus, Sneavar Gretarson and Björn Thorén for sharing your knowledge with us.

Johan Nilsson and David Oljelund, Gothenburg, June 2022

Contents

1
Introduction

This project is part of an overarching goal to reformulate ISO 5349, which is an international standard that serves to reduce vibration and improve occupational health, such that it also encompasses high frequency mechanical waves above 1250 Hz.

1.1 Background

In Sweden it is estimated that around 330 000 workers (6 % of the total active work force) use vibrating hand-held tools with an exposure of at least 2 hours per day [1]. Various diseases/injuries that affect blood vessels, nerves, joints, bones, muscles or connective tissue in the hand and forearm are connected to the use of vibrating hand-held power tools. However, the specific cause of injury in the aforementioned body parts, in terms of magnitude, frequency, duration of daily and cumulative exposure of vibration, is not yet fully understood [2].

The international standard ISO 5349 is used to guide the uses and design of vibrating hand-held tools in order to minimize the transmission of harmful vibrations to human beings. Currently, ISO 5349 is formulated to consider the frequency span 6.3 – 1250 Hz. The reasoning behind this span is based on the assumption that injury caused to the fingers is connected to the ability to sense the vibrations [3]. Within the frequency span adverse effects of hand-transmitted vibrations, depending on acceleration, frequency, cumulative and duration of exposure, can be predicated. However, for repeated impact (shock) excitation with frequencies above the specified range, ISO 5349 is only provisionary. A shock excitation is a transient (short lived) physical phenomenon which is a sudden acceleration of particles caused by an external force. It is explicitly stated in ISO 5349 that: ***"The time dependence for human response to repeated shocks is not fully known. Application of this part of ISO 5349 for such vibration is to be made with caution"*** [2].

1.2 Motivation

ISO 5349 makes up the foundation of how pertinent legislation and directives (such as the EU Vibration Directive [4]) is formulated to protect workers on a national level in multiple countries across the globe. Legislation which in turn dictates if an injured worker can claim a possible monetary compensation due to the contracted vibration related injury [5][3].

When applying the standard, an accelerometer is placed where the hand is in contact with the source of vibration such that the acceleration is measured in one out of three standardized directions. Measurements should, if possible, be done for three orthogonal directions to capture the total content of acceleration transmitted to the hand(s). Each signal from the accelerometers is filtered through a predefined band-limiting and frequency weighted filter, see Figure 1.1, by which the magnitude of the vibration is reduced by a weight factor tied to each specific frequency. An RMS (Root-Mean-Square) value of the filtered signal is calculated to represent a total magnitude of acceleration transmitted to the hand(s) in the measured direction.

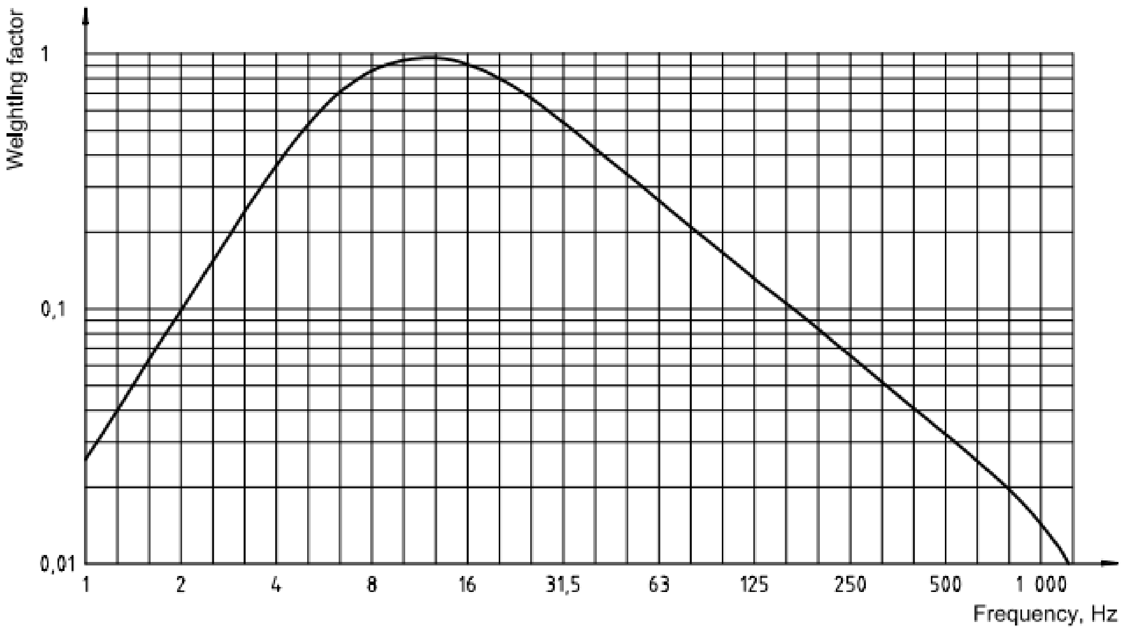

Figure 1.1: A weight factor depict how much a certain frequency is assumed to contribute to possible injury. The maximum weight factor is found in the frequency span $8-16$ Hz. For increasing frequency the weight factor decreases and at 1250 Hz the weight factor is approximately 1 % [2].

The filtering and RMS operation imply and warrant the conclusion that the impact of acceleration is insignificant for higher frequencies. The weight factor also implies that the majority of the most harmful frequencies lies in the interval $8-16$ Hz.

In spite of ISO 5349 being applied, injuries caused by vibrating power tools are still the most common occupational injury, where Hand Arm Vibration Syndrome (HAVS) is the most common work-related injury [6]. HAVS characterizes as a damage to blood vessels and nerves in the fingers and causes chronic pain, reduced sense of temperature and difficulties to perform precision work, like button a shirt [5].
Conclusively, (i) ISO 5349 is provisionary in its application regarding high-frequency vibration and (ii) the filtering removes all frequencies above 1250 Hz. These two factors, in combination with the commonality of occupational vibration-related injuries,

pose a question whether high-frequency transient vibrations could cause permanent damage and serious injury. Therefore, ways to examine and assess if high-frequency vibrations are harmful to human tissue is needed in order to complement ISO 5349. One way to examine the effects inside a finger of such waves are through FE modelling. At RISE, a 2D FE model [3] of a human finger is being developed with the aim to provide evidence that either support or disprove the claim that high-frequency vibrations cause harm.

1.2.1 Goal

The main goal of this project is to improve an existing 2D FE model, see Figure 1.2, that has been developed at RISE. To support the improvements experiments will be conducted on equipment provided by RISE. The experiment will be performed with real human fingers that will have three different treatments to study the effect of the fingerprint on the dynamic response. Any improvements suggested to the existing 2D model will be supported by experimental data that are generated during the project.

With knowledge gained from the conducted experiments a 1D FE model will be developed. The intention of the 1D FE model is to examine the characteristics of propagating mechanical waves inside the finger as a function of the material parameters, geometry and FE-mesh size. The 1D FE model will be developed based on the 2D model, but the 2D model will not be used in this project. However, properties from the 2D model, such as skin layer thicknesses and material models, are preserved and transferred to the 1D model.

A subgoal for the project will be to answer whether substitute fingers could be a viable option as experiment subjects in place of real human fingers. The reasoning behind the finger-substitutes are that (i) it would reduce the complexity of the test subject that potentially could lead to an increased consistency of the measurements taken and (ii) render the FE modelling more consistent since material data of the finger-substitute would likely have less variation in its material parameters. Therefore, cylinders with diameters representative of real human fingers will be molded with different solid cores. In summary, the following questions are to be answered:

- Is the fingerprint in the 2D model necessary to capture the dynamic response?
- Is it viable to use substitute fingers in place of a real human fingers in the experiment in order to obtain more consistent data and simplify the FE modelling?
- How well does the 2D cross section function as an approximation of a real finger? Does the cross section need more details to show a similar dynamic response as the experiment?

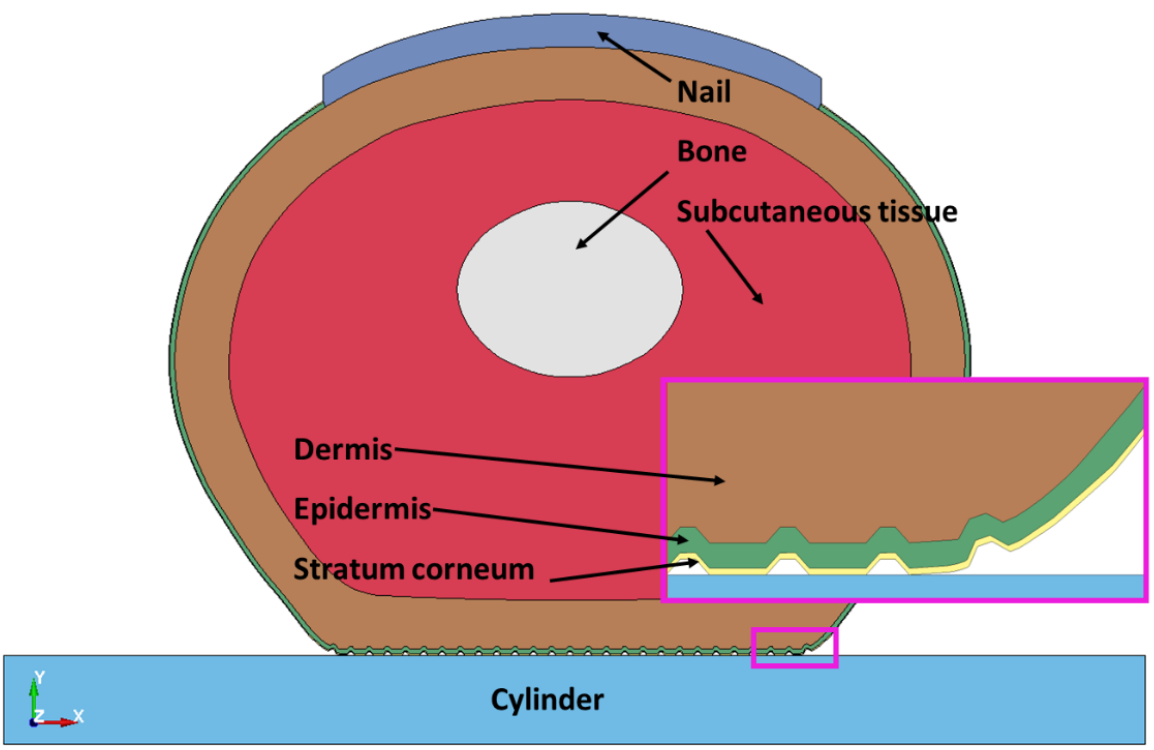

Figure 1.2: An overview showing the current 2D FE model developed at RISE. The fingerprint is visible in the pink rectangle.

1.2.2 Limitations

The complexity of the human finger and limited time makes it necessary to introduce limitations for the project.

Internal finger approximation
The 1D FE model is approximated to consist of subcutaneous tissue, bone, nail, and the three different skin layers; stratum corneum, epidermis and dermis.

Experimental data
To avoid injury to the real fingers, the introduced load in the experiments is a pulse load instead of a periodic load. The pulse load is viewed as "one period" of a continuous load. The assumption being that the affected tissue fully damps out the high frequency transients in between the impacts of a continuous load.

Wave propagation velocity
When comparing wave propagation velocity the experimental data that will be considered are loading case, fingers/specimen and hand treatment.

2
Theory and method

This chapter covers basic information on how the experiment was set up and conducted, and how the 1D FE models were developed. It also includes a brief overview of the different skin layers, software used and the finger-substitutes manufactured during the project.

2.1 Skin layers

The skin is a complex organ with many functions. It is the first line of defense against dehydration, microorganisms (infection), ultra violet light and mechanical strain. The skin is also the regulator of body temperature and the sensory organ that signals pain, temperature, touch and pressure [7].

Depending on where the skin that is examined is on the human body there are some variation in how it is built up, but in general the skin can be divided into three larger layers. A top-down order of the skin layers places the epidermis as the outermost layer followed by the dermis and subcutaneous tissue. The epidermis can be further detailed into five smaller layers; stratum basale, stratum spinosum, stratum granulosum, stratum lucidum, and stratum corneum. Where the stratum corneum is the outermost constituent [7][8]. This work has used the following division of layers: stratum corneum, epidermis, dermis and subcutaneous tissue, see Figure 2.3. Note that the fourth layer, stratum corneum has been separated out from the epidermis, see Figure 1.2.

2.2 Experiments

In this section the methodology regarding the experiments will be described. This includes the specimen used in the experiments, the setup of the experiments, and lastly the collection and processing of the signals.

To investigate if the fingerprint is necessary to capture the dynamic response different fingers with treatments to increase or decrease the fingerprint will be compared. Three aspects was taken in consideration when comparing the response of the finger print. These are the high filtered dynamic response, wave propagation velocity and max acceleration.

To investigate the alternative of using substitute finger instead of real fingers the same aspects were taken in consideration. The results of the substitute fingers were compared to the results of the real fingers.

2.2.1 Fingers and substitution fingers

The finger specimens comprised of two individuals, called A and B. Both individuals used the right hand index finger $R1$. Furthermore was different treatment on the fingers used. These treatments were neutral finger denoted by no further index, acetone treatment denoted *aceton* and electro-conductive gel denoted *blagel*.

For the neutral finger treatment was the finger not subjected to any special chemicals or gel. The acetone treated finger was saturated with acetone to remove dirt, grease and moisture from the fingerprint. The assumption being that the topology of the fingerprint got fully exposed. For the electro-conductive gel treated finger was the finger saturated with electro-conductive gel. The assumption being that the cavities in the fingerprint got filled by gel, thus fully remove the effect of the fingerprint.

The substitution fingers were made of a combination of material chosen to substitute different part of the fingers. The soft part of the finger such as the different skin layers, flesh, nerves and blood vessels were grouped together into the one material and substituted by a hyper-elastic material. The materials chosen were ballistic gel and silicone rubber. The bone was substituted by elastic materials. These materials were chosen to be wooden, polymethacrylate (PMMA) and stainless steel. The geometry of the substitution fingers were made as cylinders with different specified dimensions.

The substitute fingers were produced by inserting the different substitution materials into specialised molds. The molds were produced by 3D-modeling in `CATIA v5` and additive manufacturing by a `FLASHFORGE FINDER` 3D-printer.

The tissue part of the specimen was made into cylinders with three different diameters. These diameters were chosen to be 12 mm, 16 mm and 24 mm. The length of the tissue part of the specimen specimen was set to 100 mm.

The bone substitute material was cut into pieces of 150 mm. The mould was formed to allow the bone substitute to stick out 10 mm on one side of the specimen and 40 mm on the other side.

The ballistic gel material was produced from `BALLISTICGEL` [9]. The total volume produced was 0.25 L. The portion of `BALLISTICGEL` powder was 0.05 L and the portion of water was 0.2 L. The ballistic gel was mixed in room temperature (around 20°C) and was left to harden for 48 hours in a temperature of around 4°C before removal from the molds.

The silicone specimen were moulded from the same batch of silicone. The silicone material used was a mix of `ELASTOSIL® RT 607 A` and `ELASTOSIL® RT 607 B`, where the latter is the hardening to start the hardening process of the silicone. The total volume produced was 1.2 L. The portion of hardening material of the total volume was 1/10 i.e. 1.08 L `ELASTOSIL® RT 607 A` and 0.12 L `ELASTOSIL® RT 607 B`. The material was left to harden for 24 hours before being removed from the molds. The silicone was mixed and left to harden in room temperature (around 20°C).

In Figure 2.1 three of the ballistic gel specimen and three of the silicone specimen can be seen.

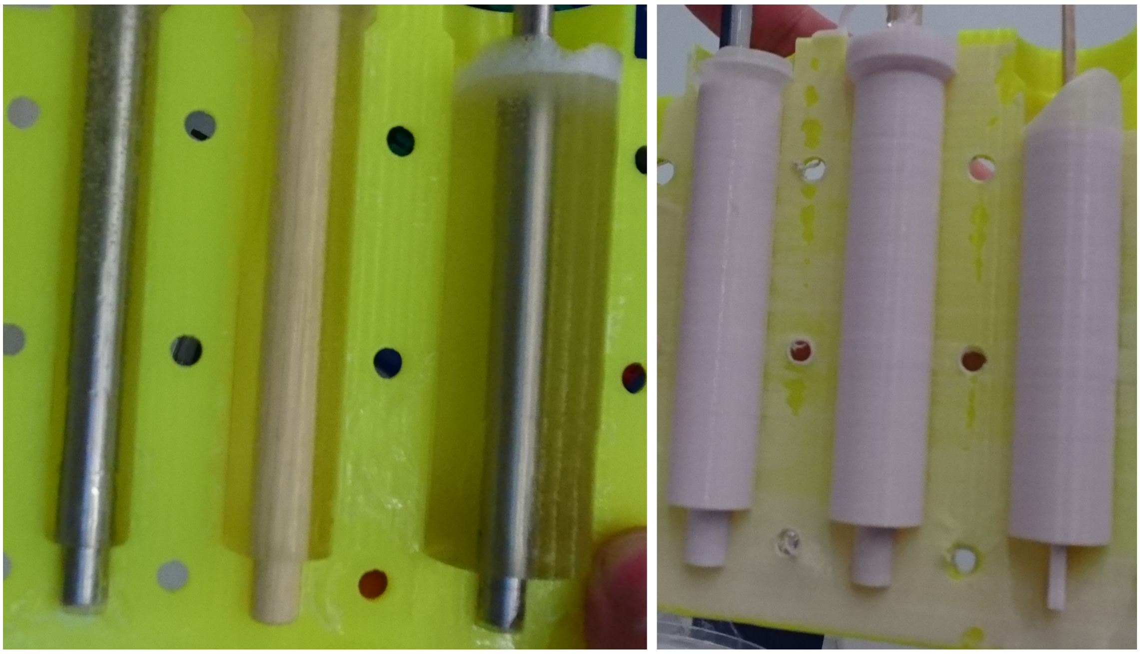

Figure 2.1: Picture of three of the ballistic gel specimen (left) used and three of the silicone specimen (right) used.

In Table 2.1 can the data for the specimen tested be seen.

Specimen	**Diameter [mm]**	**Person**	**Treatment**	**Bone substitute**	**Tissue substitute**
AR1	11.5	A	–	–	–
AR1_Aceton	11.5	A	Acetone	–	–
AR1_Blagel	11.5	A	ECG	–	–
BR1	10.6	B	–	–	–
BR1_Aceton	10.6	B	Acetone	–	–
BR1_Blagel	10.6	B	ECG	–	–
B1S1	12.0	–	–	Wood	Ballistic gel
B1S2	16.0	–	–	Steel	Ballistic gel
B1S3	24.0	–	–	Steel	Ballistic gel
B1S4	12.0	–	–	Steel	Ballistic gel
B1S5	16.0	–	–	Wood	Ballistic gel
B2S1	12.0	–	–	Wood	Silicone
B2S2	16.0	–	–	Wood	Silicone
B2S3	12.0	–	–	PMMA	Silicone
B2S4	16.0	–	–	PMMA	Silicone
B2S5	16.0	–	–	Steel	Silicone
B2S6	16.0	–	–	Steel	Silicone

Table 2.1: Specimen data for the tested specimen. ECG is denoting electro-conductive gel.

2.2.2 Experiment setup

The experimental setup consisted of a test rig to instiating the load of the specimen and a Laser Doppler Vibrometer (LDV) to measure the response.

In Figure 2.2a a photo of the experimental setup can be seen and in Figure 2.2b a schematic of the experiment setup is shown.

The experimental setup used was built around a structure of aluminum profiles. The profile structure was mounted on wheels and fixed in horizontal direction to the ground with a dynamometer between. The dynamometer therefore measured the total horizontal force applied to the beam structure. The impulse on the specimen was generated by releasing a small hammer from a number of fixed positions. These positions were identified by the angle between the arm of the hammer and the vertical axis. The hammer was attached to the beam structure as a pendulum. The angle the pendulum was dropped from was controlled by a stop pin that could be placed to ensure the right angle was achieved. When the hammer was released it stroke a steel cylinder attach to the beam structure through sylomer material. The different specimen were placed on the opposite end of the cylinder with a chosen set of forces pointing horizontal towards the steel cylinder. A force sensor was attached to the hammer to measure the striking force applied onto the cylinder.

The LDV was directed normal to the cylinder surface to measure the horizontal response of the specimen. The measurements were performed 1 cm from the end of the finger nail for the finger specimen and 1 cm from the edge of the specimen for the substitute specimen. To ensure that the laser reflection was sufficient small reflective marbles were glued to the specimen. There was only one LDV available which meant that the input on the specimen and the output of the specimen could not be measured at the same time. The specimen input was therefore measured on separate loading instances from the specimen output. The specimen input was measured directly on the cylinder surface for the different load cases.

A consequence of the way the hammer was released before striking the cylinder introduced an external horizontal force. The actual force of the specimen is therefore different to the force seen on the dynamometer. The mass of the hammer was 0.12 kg and the mass of the rest of the setup was 15.60 kg, thus the dynamic horizontal force is assumed to be zero. The derivation of the static horizontal force compensation is given in Appendix A.1.

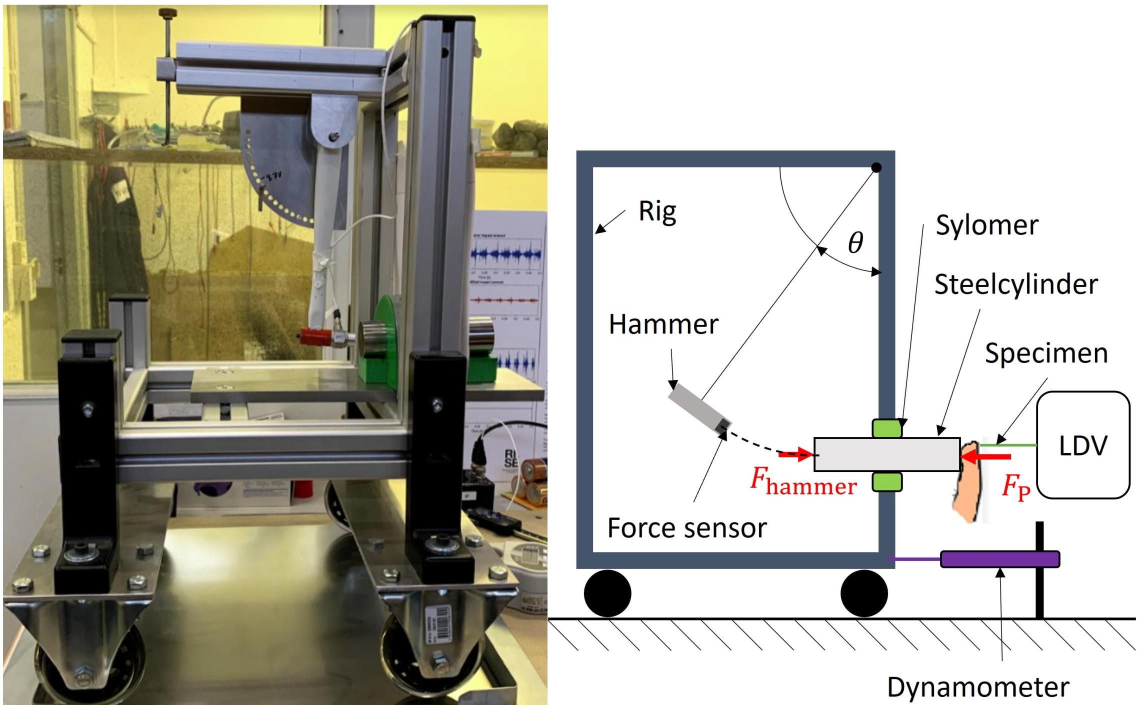

(a) Photo of the experimental setup used [10].
(b) Schematic of the experiment setup.

Figure 2.2: Photo and schematic of the of the experimental setup.

The fixed positions for the hammer were given by the angle θ that was set to, 90°, 60° and 45°. The force measured on the dynamometer just before releasing the hammer were 4 N and 10 N. The combination of the position of the hammer and force on the dynamometer was the load case for the experiment.

The load cases tested for the experiments can be seen in Table 2.2.

Load case	**Hammer angle [degrees]**	**Force [N] (Dynamometer)**	**Force [N] (Actual)**
P1D1	90	4	4
P1D2	90	10	10
P2D1	60	4	3.32
P2D2	60	10	9.32
P3D1	45	4	2.82
P3D2	45	10	8.82

Table 2.2: Load cases for the specimen tested in the experiments.

2.2.3 Data collection process

The experiments were conducted for different specimens at different dates. Some specimen were tested only on one date and other on more than one date. Each test was repeated four consecutive times for the same load case. This were done to be able to observe the repeatability of response and any abnormalities.

The software LabView was used to monitor and save data from the different experiments. The force sensor on the hammer was used to start the recording of the signal response by constantly measuring the force and start saving when it measured a high impulse. The sampling rate of the LDV were set to 1MHz.

To make sure whole of the first impulse effect was collected, data for 1 ms before the impulse was saved. This included the whole wave propagation in all different specimen. Additionally a consequence of the force vector measuring the force on the hammer was the response displaced in time by the wave propagation in the cylinder. To make sure the whole impulse effect were collected were 50 001 samples saved for each test.

2.2.4 Dynamic response

To study the high frequency part of the collected data, it was necessary to filter the signal. All the velocity and acceleration signal responses were filtered through a Butterworth high pass filter of the 6th order. The cut-off frequency of the signal was set to 1000 Hz. This was done to make sure the whole signal over 1250 Hz would remain in the filtered signal. All signal processing was performed using `MATLAB`. For the high pass filter the commands `butter` and `filtfilt` was used.

2.2.5 Wave propagation velocity

From the experiment only the input form the cylinder response and the output of the specimen could measured. The wave propagation velocity through the specimen could therefore only be derived as a mean over the specimen. Furthermore can the LDV only measure the longitudinal wave and not the transverse waves. Therefore was only the longitudinal wave considered for the wave propagation velocity. The length of the specimen divided by the difference in time between the input signal and output response of the specimen will give the mean wave propagation velocity.

The method to derive the time difference is to compare the time between the initial input signal on the specimen, which will be the cylinder response, and the initial response of the specimen signal. In practice it was necessary to find the same stages of the impulse in the cylinder and specimen responses to make sure it represents the time difference difference, Δt in time between velocity of cylinder, t_{cylinder} and specimen, t_{specimen}. The point chosen was therefore at the time when both signals get the first initial impulse in their velocity response, after the first 1000 time steps, i.e.

$$\Delta t_{\text{case}} = t_{\text{specimen}} - t_{\text{cylinder}} \ . \tag{2.1}$$

There will be a time lag in the measurement due to both a time displacement from the LDV and the data collection process. However, in the time difference, Δt the time displacement will be eliminated because this time displacement was present in all signals, included the cylinder signal.

The specimen length that the wave propagates through was assumed to be the undeformed diameter. The specific sample diameter was then divided with the time difference to give the wave propagation velocity

$$v_{\text{sample}} = \frac{D_{\text{sample}}}{\Delta t_{\text{case}}} \ . \tag{2.2}$$

2.2.6 Max acceleration

The max acceleration was derived by identifying the max amplitude of the high passed dynamic acceleration response. This was done for each measurement. The span for different specimen and load cases were then plotted and compared by statistically test.

2.2.7 Statistical test

The interval of different specimen, load cases and dates for wave propagation velocity and max acceleration was then studied.

This included comparison by the use of Levene's test. The Levene's test is a statistical test to compare variances in grouped test data for different samples. The null hypothesis is that the variances are the same for all groups of samples. The differences of variances between the groups of samples are then compared to each other, which is presented in form a p-value. If the p-value is higher than a chosen factor of significant (usually p=0.05) then the variances in the groups of samples for the different specimen are considered not significantly different to each other. Otherwise if the p-value is lower than the factor of significant, then the variances in the groups of samples for the different specimen are considered significantly different [11].

2.3 Computational methodology - 1D FE model

In this section the necessary inputs can be found to set up the 1D model used in the project. The project has utilized LS-PrePost [12] as the software to develop the 1D FE models. To set up calculable FE models LS-PrePost uses keyword input, these will be referred as *< `SOME_KEYWORD` >, more info about this can be found in [13].

2.3.1 1D model setup

The pre-processing part includes model geometry, mesh, material parameters, loads, damping and boundary conditions.

2.3.1.1 Geometry

Two different geometry settings was used in the project, which were named the **real** geometry and the **homogeneous** geometry. The real 1D geometry constructed were chosen such that it would both represent the previously developed 2D model. This in terms of dimension and how the experiment setup of how the LDV was positioned when the dynamic response of the nail was measured. Therefore, the real 1D model was chosen on the vertical symmetry line of the 2D model. The same arguments were applied for the homogeneous geometry where the only difference was that it had the same thickness for all the layers synthesizing the column. Each resulted in a column consisting of a total of ten layers of nail, bone and soft tissues. A sketch of the column can be seen in Figure 2.3.

Total length	14.1 mm
Nail	0.5 mm
Stratum corneum	0.025 mm
Epidermis	0.1 mm
Dermis	0.3975 mm
Subcutaneous tissue	1.6 mm
Bone	4.5 mm
Subcutaneous tissue	6.0 mm
Dermis	0.875 mm
Epidermis	0.1 mm
Stratum corneum	0.025 mm

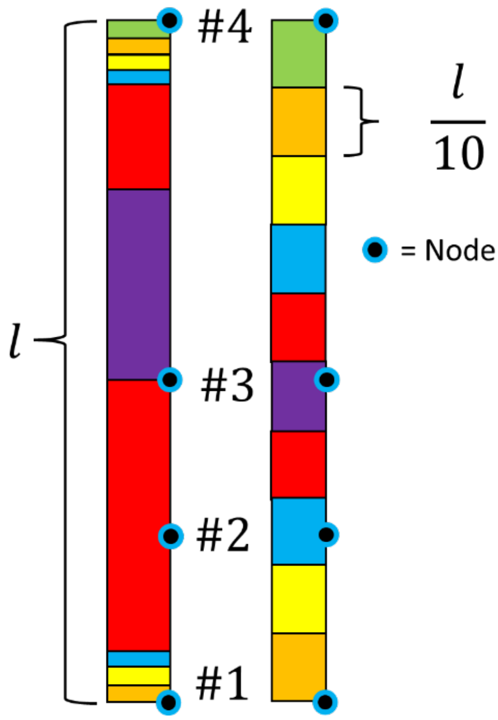

Figure 2.3: Sketch of the real geometry to the left and the homogeneous geometry to the right. NB! The models are not to scale. The numbered black and blue circles show positions of nodes where measurement were taken. The coloured table to the left have the dimensions of each layer of the real layer, where l is the total length of the two columns.

2.3.1.2 Mesh and material models

Standard plain strain elements were used for all developed FE models. Soft tissues were modelled with the material card `*MAT_VISCOELASTIC` [14]) and the nail and bone with `*MAT_ELASTIC` [14]).

2.3.1.3 Material parameters

The material parameters used were taken from [3], [15], [16] and [17] which have been used in previous work at RISE. Bulk modulus and density have been kept equal for the soft tissues, i.e. skin layers and subcutaneous tissue, since these do not differ significantly [3]. Additionally, there will always be a reflection and transmission at the boundary between two materials with a difference in density [18]. Therefore the assumption of negligible reflection was made for the soft tissues and attention was focused on the material parameters of the bone. Table 2.3 shows the material parameters of bone that have been implemented in the FE-model.

Material parameters	
Density 1 $-\rho_1$	1000 [kg/m^3]
Density 2 $-\rho_2$	1600 [kg/m^3]
Density 3 $-\rho_3$	1960 [kg/m^3]
Bulk modulus $-K_1$	10000 [MPa]
Bulk modulus $-K_2$	20000 [MPa]
Bulk modulus $-K_3$	30000 [MPa]

Table 2.3: Material parameters used for the bone.

2.3.1.4 Load

The load, applied at node 1, used for the 1D FE models has been either been a scaled version of Figure 2.4a, where the curve was scaled with frequencies 10, 100, 1000, 10 000, 20 000 and 50 000 Hz or the real input curve in Figure 2.4b. The real input curve was measured on the cylinder while a finger applied a force of 4N, which was implemented without scaling.

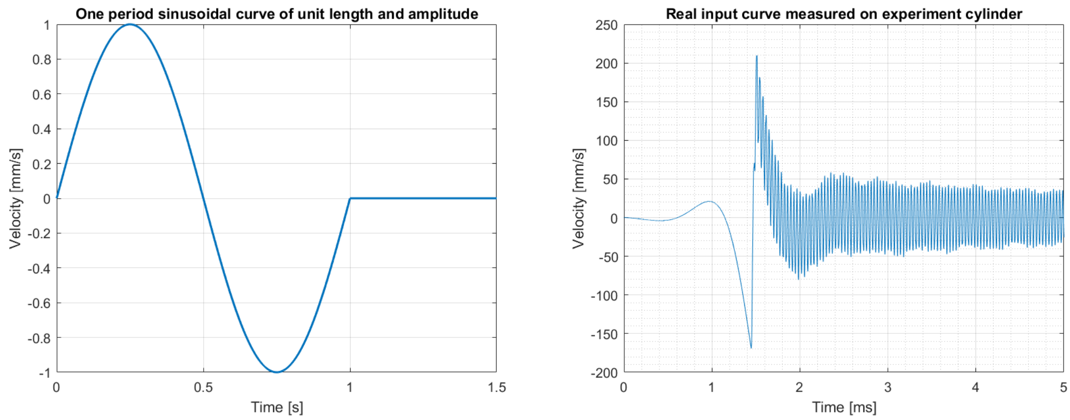

(a) One period unit sinusoidal curve padded with zeros after one period.

(b) Real input velocity curve.

Figure 2.4: Implemented load curves where (a) is a pure sinusoidal curve without high frequency oscillations and (b) is a signal measured on the steel cylinder of the experiment.

2.3.1.5 Damping

In LS-DYNA implementing damping to the structure was optional and many sophisticated alternatives of how to impose damping were available [19]. The desired outcome was to obtain the maximum value of the velocity output produced by the 1D FE model such that it stayed within an interval defined by the maximum and minimum velocity value from experimental data seen in Figure 2.5. The damping coefficients and selection of the available damping schemes (`*DAMPING_PART_MASS_SET` and `*DAMPING_PART_STIFFNESS`) were therefore implemented through trial and error in an effort to try match the experimental curve. In general the `*DAMPING_PART_MASS_SET` applies more to low frequency waves and rigid body motion, and the *DAMPING_PART_STIFFNESS applies more to the high frequency waves, further in-depth details can be found in [19]. These two damping methods were implemented to the 1D FE model, where the third option was active for both cases.

1. The first case of damping used the keyword *DAMPING_PART_MASS_SET where a constant damping of $1.0 \cdot 10^6$ was added to the bone.
2. The second case of damping used the keyword *DAMPING_PART_MASS_SET where a constant damping of $1.6 \cdot 10^6$ was added to the bone and $1.4 \cdot 10^6$ to subcutaneous tissue, epidermis and stratum corneum.
3. For both cases of damping the *DAMPING_PART_STIFFNESS keyword was active for all parts in the model with a COEF=0.9.

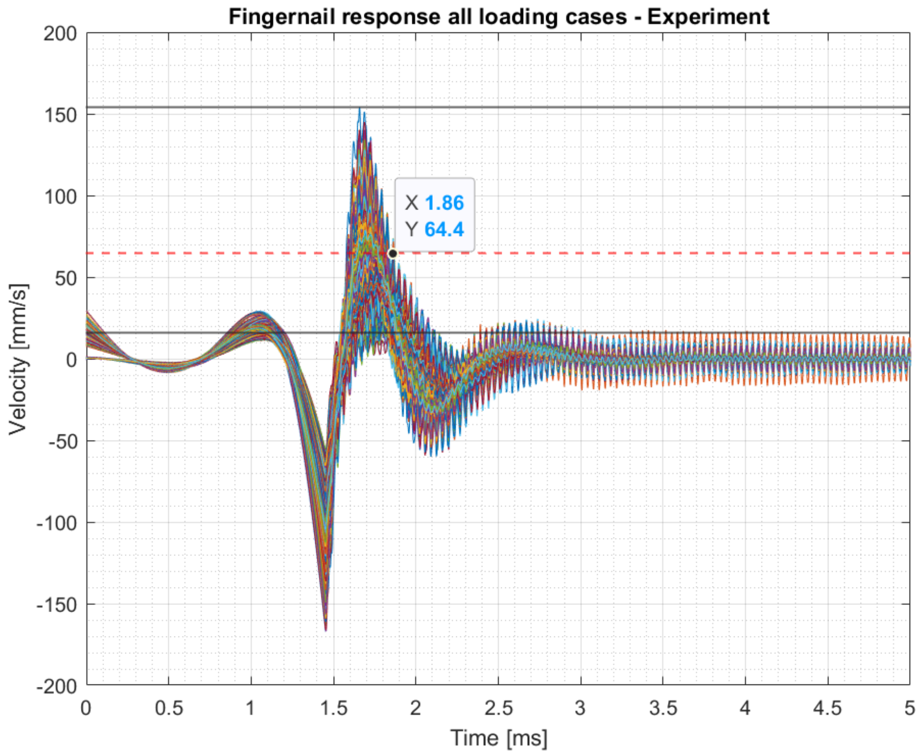

Figure 2.5: In the plot all the output signals from the experiment are presented. The two black horizontal lines correspond to the maximum and the minimum value. The dashed line is the mean value of all the maximum peak values.

2.3.1.6 Boundary and initial conditions

The models were constrained to only translate in one direction and the loads were prescribed as velocities directly onto nodes at position 1 in Figure 2.3.

2.3.1.7 Output sampling rate

To rule out aliasing frequencies the Nyquist criteria [20] was applied. According to unpublished LS-DYNA support recommendations an output sampling rate of that at least 4−6 times the frequency of interest should be considered. Still, 10 MHz was opted for since this gave a good resolution of the output.

2.3.2 Simulation and data extraction

Here follows information about the different simulations made to the 1D FE model and how information were extracted.

2.3.2.1 Mesh convergence

To study whether the ability of the mesh from the 2D-model was able to resolve mechanical waves with frequencies between 10 − 50 000 Hz a mesh convergence study was conducted. The mesh was uniformly refined at each step, each step reduced the element size by half. That procedure was repeated until the difference in wave propagation velocity between mesh sizes where small and/or there was a visible convergence, see Figure 4.1 for a visual exposition. The outcome of the convergence study determined the mesh sizes used in the project.

As the only exception, material parameters used in the mesh convergence study differs from what has been previously stated, see Table 2.4. This is in part to check the previously used materials from [3] and to be able to compare these with the experimental data. The quantity measured was wave propagation speed, c, therefore the material parameters of interest were the bulk modulus, K, and the density, ρ, since wave propagation speed is decided by the relation

$$c = \sqrt{\frac{K}{\rho}}. \tag{2.3}$$

Material parameters	K [MPa]	ρ [kg/m^3]
Soft tissues	2190	1000
Bone	18 333	1960
Nail	1933	1330

Table 2.4: Material parameters used in the mesh convergence study.

2.3.2.2 Geometry and dimension

To examine the importance of the geometry in the pertinent 1D FE model was set up with the same thickness of the constituent layers, see the right-hand column in Figure 2.3. The two models were then run with the exact same material parameters, mesh size, load and boundary conditions. The nodes used for measurement were the same coordinates for the real and homogeneous geometries. The curves produced at the nodes of interest was then compared for the two cases.

2.3.2.3 Wave reflection

To study how the different combinations of bulk modulus and density affected the dynamic response within the finger and at the nail (nodes 2 and 4), the real geometry model was set up for all layers with the same density, bulk modulus and material model. The load applied was a wave load with frequency of 1600 Hz and a amplitude of 1.6 [m/s] given by a curve based on the lower frequency of a real input curve.

A reference curve was extracted from the homogeneous model in which the propagating wave moved without interference. In a second part of the test bone was added to the model with a linear elastic model. This model was tried for all the nine combinations of material parameters and the differences between those curves and the reference curve were examined.

2.3.2.4 Real input

The curve in Figure 2.4b was used as input to the 1D FE model. The FE model was run for the two cases of damping previously described and with the nine different combinations of material parameters for the bone given in Table 2.3. Curves produced from these two settings of damping and the nine combinations of material were then plotted in both the time and frequency domains.

3
Results

In this chapter results from experiments and FE-model are presented.

3.1 Experiment

The results derived and analyzed from the experiments are the dynamic response of the specimen, the mean wave propagation velocity and maximum acceleration.

3.1.1 Dynamic response

The dynamic response of the specimen consists of velocity response and acceleration response. In Figure 3.1 the high pass filtered velocity response and acceleration response for all fingers, ballistic gel and silicone molding compound specimen, for all load cases for the the first 6 ms can be seen.

The high pass filtered finger specimen velocity response, regardless of person, loading case and the date of when the experiment was performed has a clear dominant lower frequency with higher frequency oscillations. The amplitude of both the lower frequency and the oscillation differs significantly from each other which indicates some variations between the fingers that depend on either the specific finger specimen, on the loading case or on factors that change between different dates.

The high pass filtered ballistic gel specimen response for load case and the date of when the experiment where performed has no visible similarity in the dynamic response that is the same for all specimen. The response consists of short impulses with high amplitudes and high frequency oscillations. However these impulses have varying amplitudes and occur phase shifted from each other. This implies that the dynamic response for ballistic gel specimen is dependent of either the specimen variation, loading cases or factors that changes from different dates. Due to breaking of the ballistic gel specimen, as pressure was applied during the experiment, not all loading cases could be tested for all specimens.

The high pass filtered silicone specimen response for the load case and the date of when the experiment was performed have some resemblance of an general dynamic response that is similar for all specimen. By general dynamic response it is meant that there is a visible lower frequency with higher frequency oscillations. However the amplitude varies notably between the different specimens and some phase shift seems to be present. This means that the dynamic response is dependent on either specimen variation, on loading cases or on factors that change between different dates.

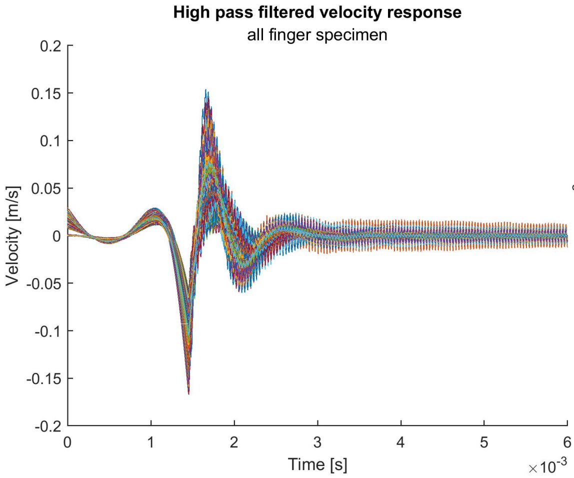

(a) Finger, velocity.

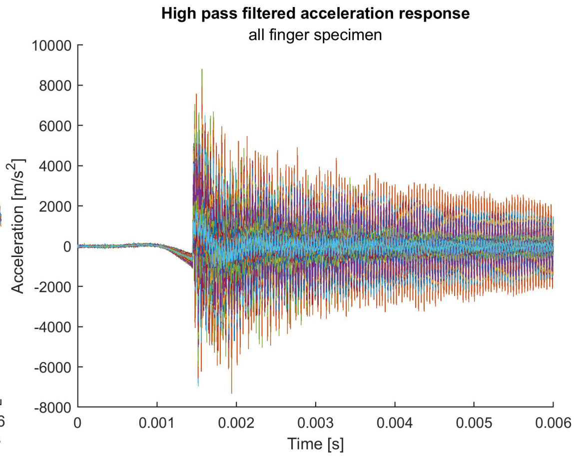

(b) Finger, acceleration.

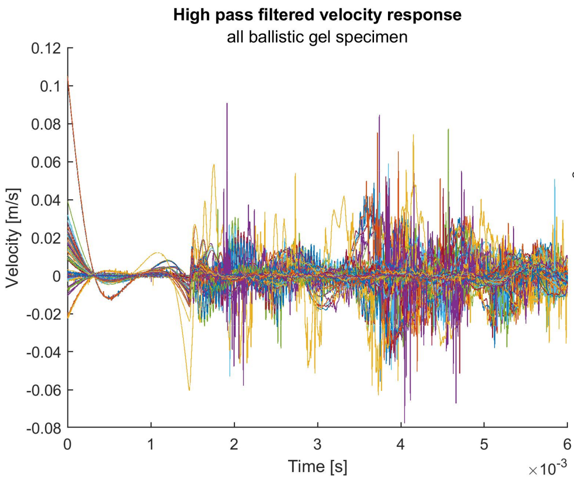

(c) Ballistic gel, velocity.

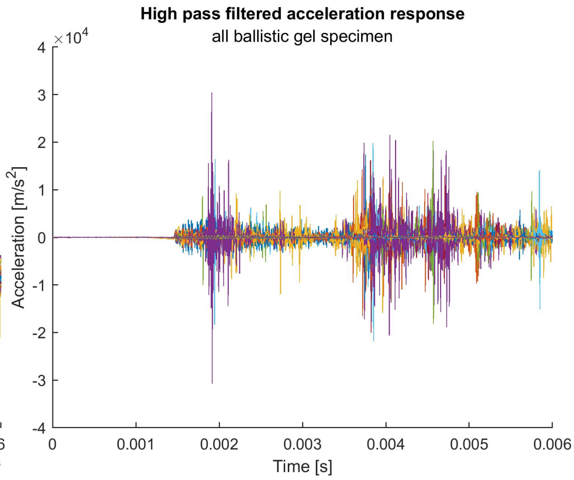

(d) Ballistic gel, acceleration.

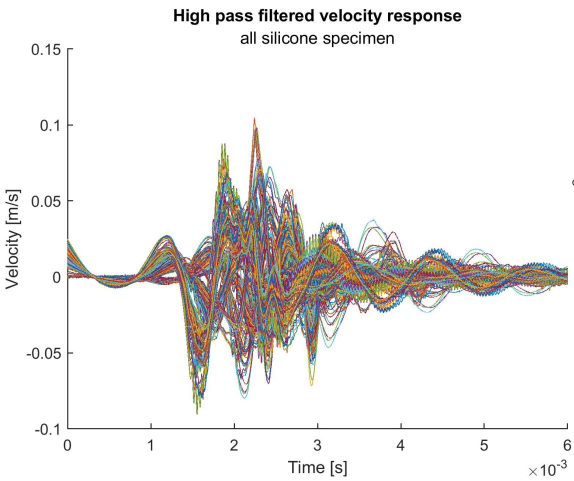

(e) Silicone, velocity.

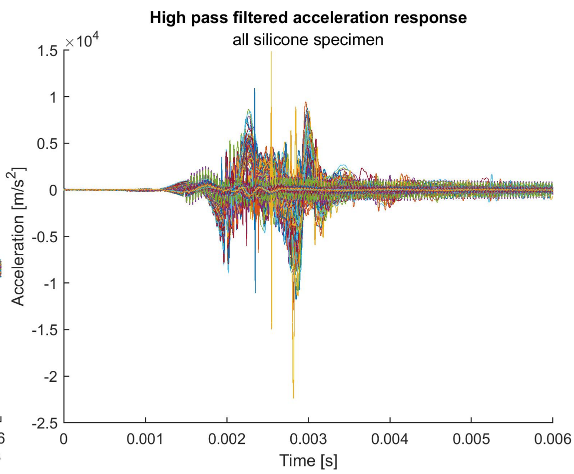

(f) Silicone, acceleration.

Figure 3.1: High pass filtered velocity and acceleration response for all fingers, ballistic gel and silicone molding compound specimen for all load cases for the the first 6 ms

3.1.2 Wave propagation velocity analysis

The wave propagation velocity for the experimentally gathered data was analysed. The analysis included a comparison of different load cases for the same specimen and between groups of specimens of the same type, such as fingers, ballistic gel and silicone molding compound. Furthermore a comparison between the different types of specimen. Lastly the difference between the type of treatments of the finger surface, such as application of acetone and electro-conductive gel.

The measured specimen results were combined into groups for each individual specimen and each individual loading case, independently of date or time the experiment were performed. Levene's test was then preformed for each specimen and their different loading cases.

First the finger specimen is considered. In Figure 3.2 the finger specimen are combined into groups for each individual loading case independently of date can be seen.

The variances between the loading cases for each individual specimen were not significantly different according to Levene's test, with the exception of person A treated with electro-conductive gel and person B treated with acetone, see Table 3.1. However, for both specimen there were only one loading case each, which had a variance significantly smaller than the rest. The number of data set of samples collected for each loading case of each specimen were only 12 and furthermore the span of each loading case was inside the span of the rest of the data sets. The assumption was therefore made that the data sets for each loading case could be combined into the group of responses for each specimen.

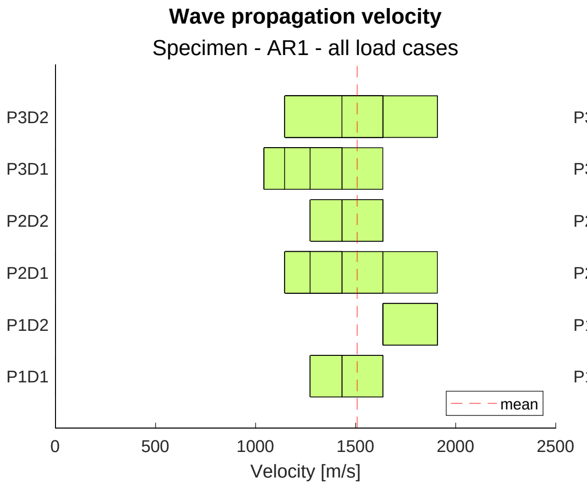

(a) Specimen $AR1$.

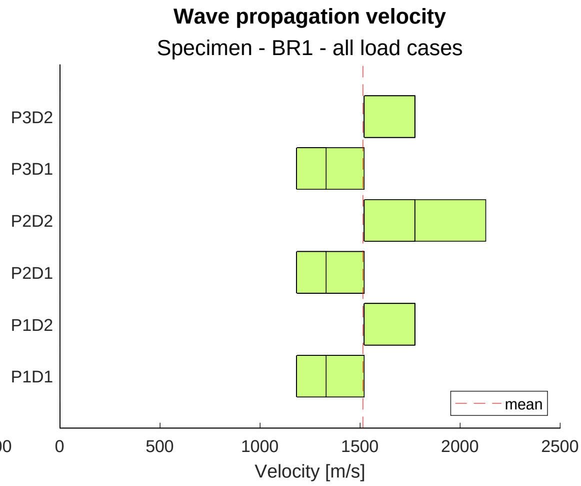

(b) Specimen $BR1$.

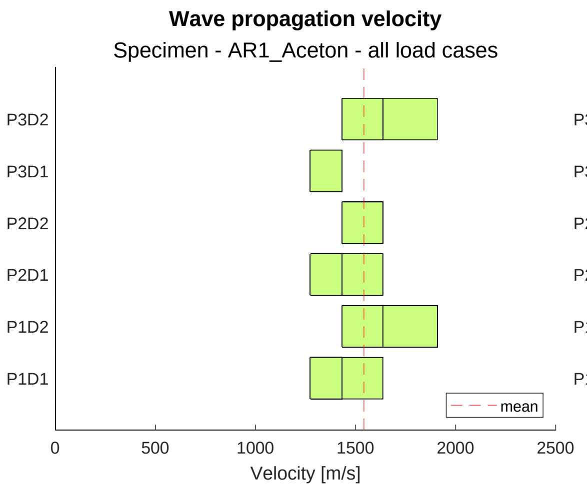

(c) Specimen $AR1\_Aceton$.

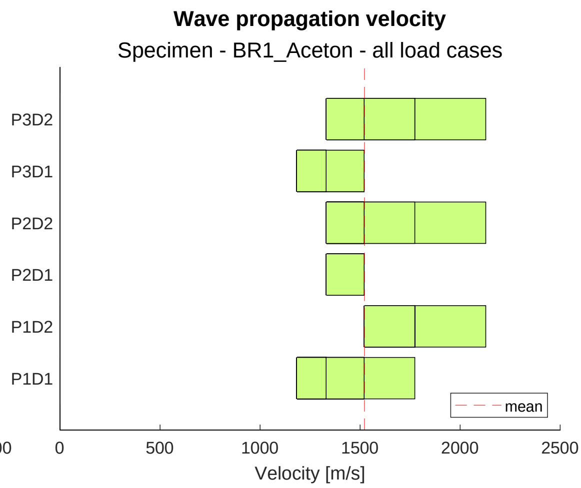

(d) Specimen $BR1\_Aceton$.

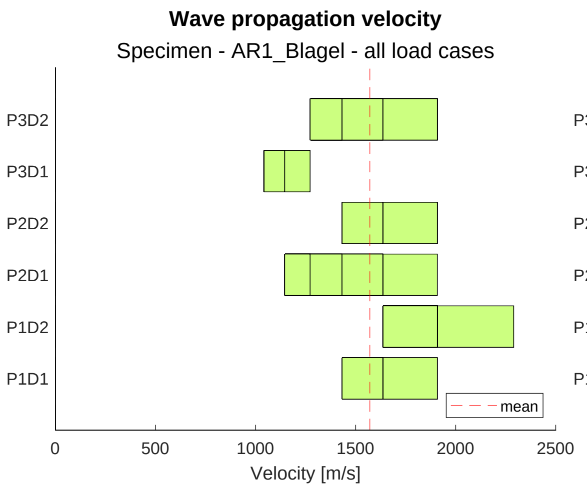

(e) Specimen $AR1\_Blagel$.

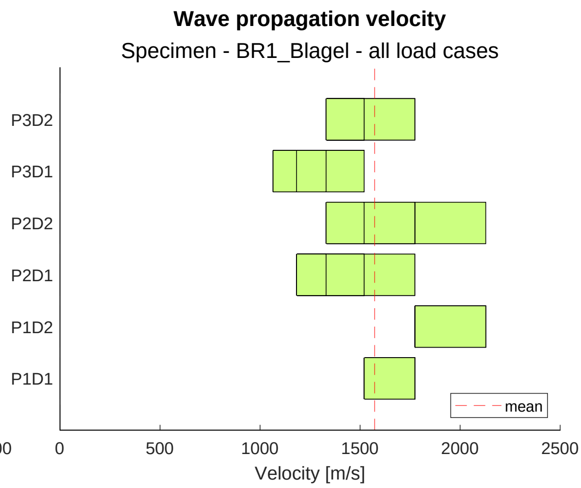

(f) Specimen $BR1\_Blagel$.

Figure 3.2: The finger specimen combined into groups for each individual loading case independently of date.

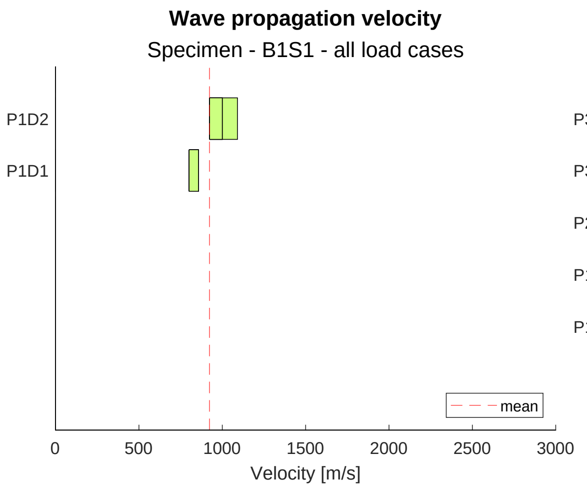

(a) Specimen $B1S1$.

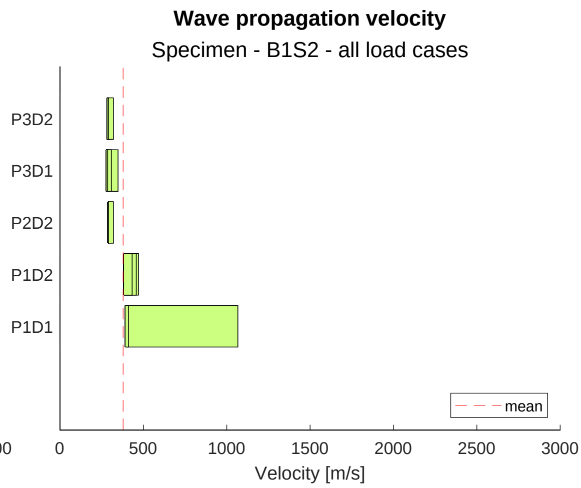

(b) Specimen $B1S2$.

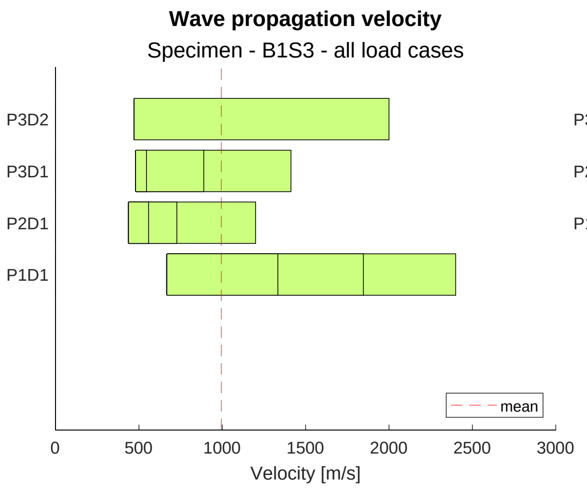

(c) Specimen $B1S3$.

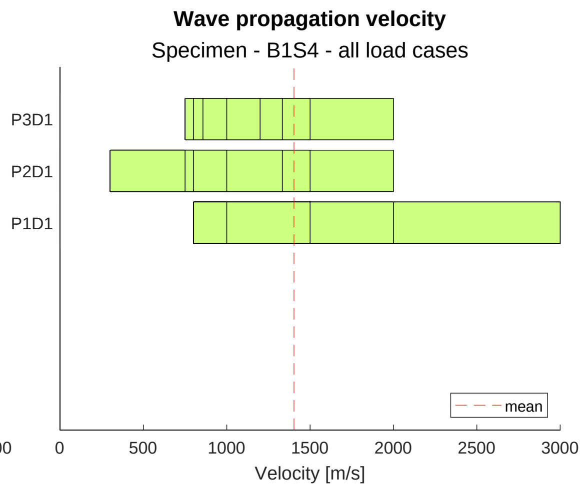

(d) Specimen $B1S4$.

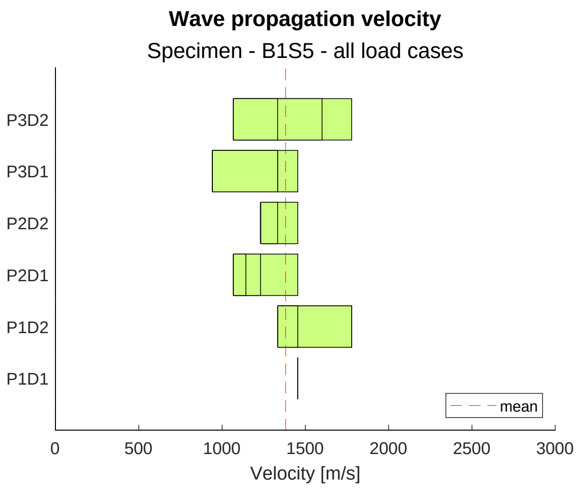

(e) Specimen $B1S5$.

Figure 3.3: The ballistic gel specimen combined into groups for each individual loading case independently of date.

Next was the ballistic gel specimen considered. In Figure 3.3 the ballistic gel specimen combined into groups for each individual loading case independently of date can be seen.

However when considering the ballistic gel specimen it should be noted that due to the ballistic gel specimen breaking during experiment the variances could not be sufficiently compared by Levene's test. The purpose of the ballistic gel specimen was to compare the response and wave propagation velocity to real fingers. The measured samples for the fingers were as previously mentioned grouped into each finger specimen. The measured samples for the different load cases were therefore also grouped the same way into each ballistic gel specimen.

Lastly was the silicone specimen considered. In Figure 3.4 the silicone specimen is combined into groups for each individual loading case independently of date can be seen.

The variances between the loading cases in all the individual specimen were significantly different to each other according to Levene's test. However, it should be noted that all the silicone specimen visually seems to have mutually similar forms. The load cases in terms of the magnitude of the input impulse seems to give similar variants in the span for all specimen. The magnitude of the wave propagation velocity is however not the same for the different specimen. Differences due to the load case is however not considered when comparing the real finger specimen. The assumption was therefore made that the measured samples for all loading cases could be grouped into each silicone specimen to enable comparison with finger specimen.

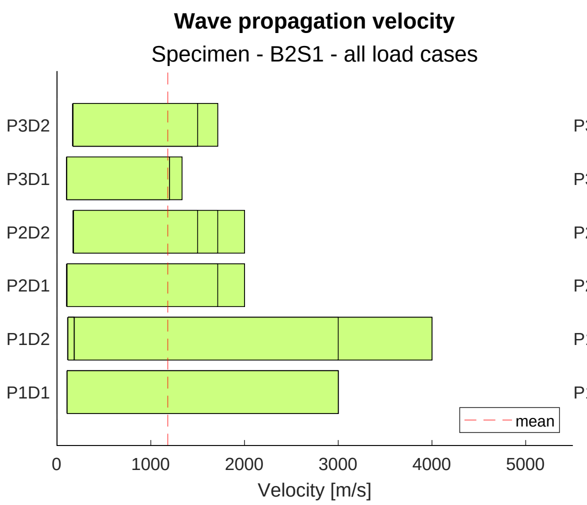

(a) Specimen $B2S1$.

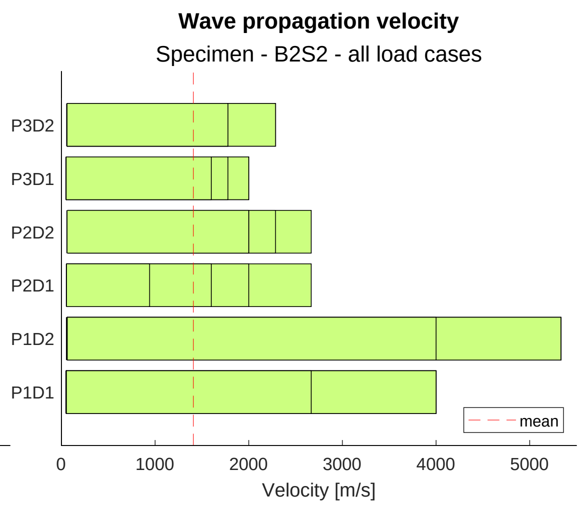

(b) Specimen $B2S2$.

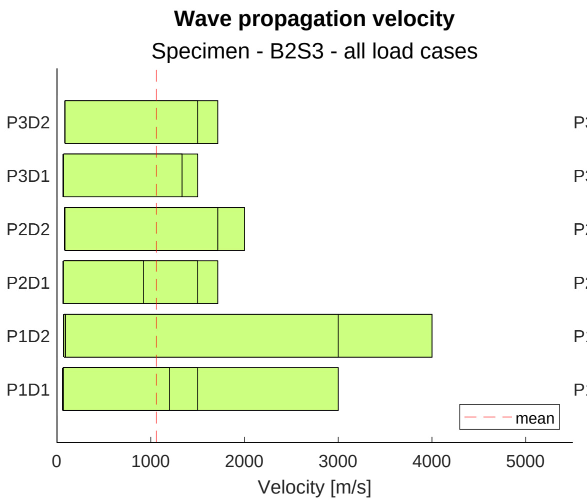

(c) Specimen $B2S3$.

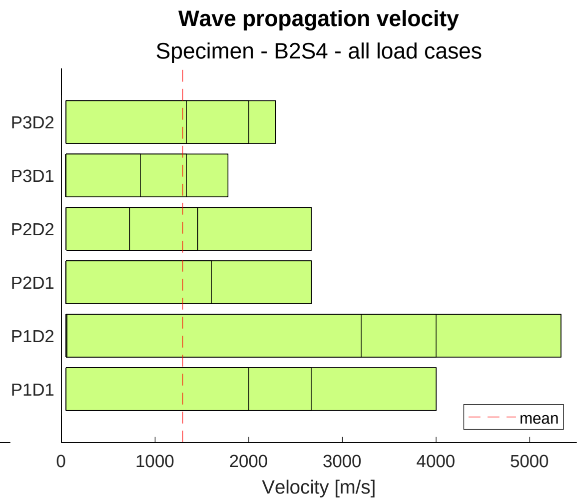

(d) Specimen $B2S4$.

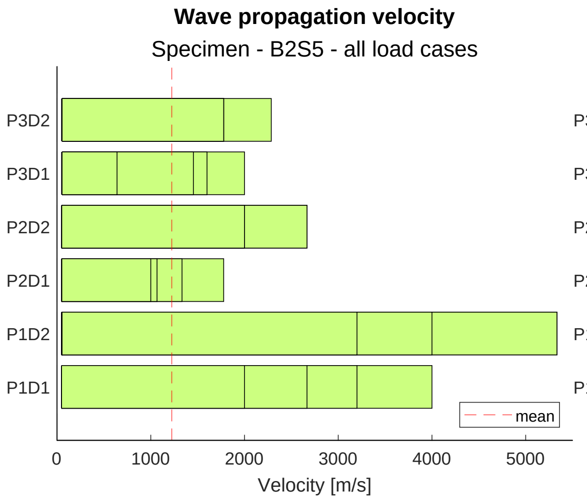

(e) Specimen $B2S5$.

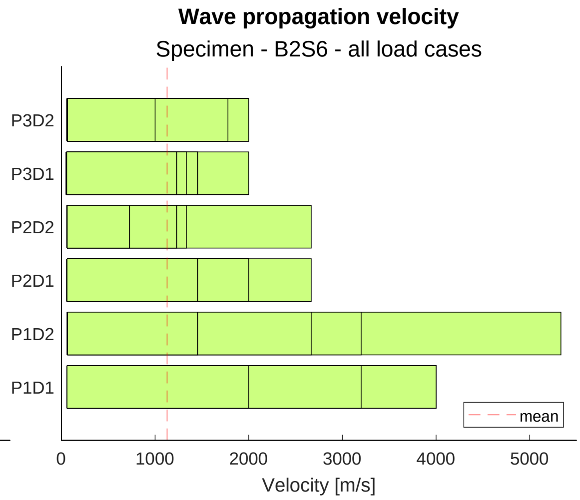

(f) Specimen $B2S6$.

Figure 3.4: The silicone specimen combined into groups for each individual loading case independently of date.

In Figure 3.5 each category of the specimens used in the all experiments has been grouped together. In Table 3.1 the mean wave propagation velocity and p-value between load cases for each specimen as well as number of data sets of samples included in each specimen and total number of samples for the different types of specimen can be seen.

Specimen	**mean WPV [m/s]**	**p-value**	**Number of samples**
AR1	1508	0.324	72
AR1_Acetone	1524	0.2031	72
AR1_Blagel	1571	0.017	72
BR1	1514	0.526	72
BR1_Acetone	1522	0.0053	72
BR1_Blagel	1573	0.216	72
Total Fingers:	1538	0.0003	432
B1S1	923	0.184	8
B1S2	379	0.0	20
B1S3	994	0.497	16
B1S4	1403	0.116	24
B1S5	1381	0.0	24
Total Ballistic gel:	814	0.0	90
B2S1	1181	0.0271	48
B2S2	1409	0.0258	48
B2S3	1059	0.0449	48
B2S4	1295	0.0478	48
B2S5	1224	0.0108	48
B2S6	1128	0.0764	48
Total Silicone:	1190	0.0477	288

Table 3.1: Mean wave propagation velocity and p-value for each specimen as well as number of data sets of samples included in each specimen and total number of samples for the different types of specimen. WPV - wave propagation velocity.

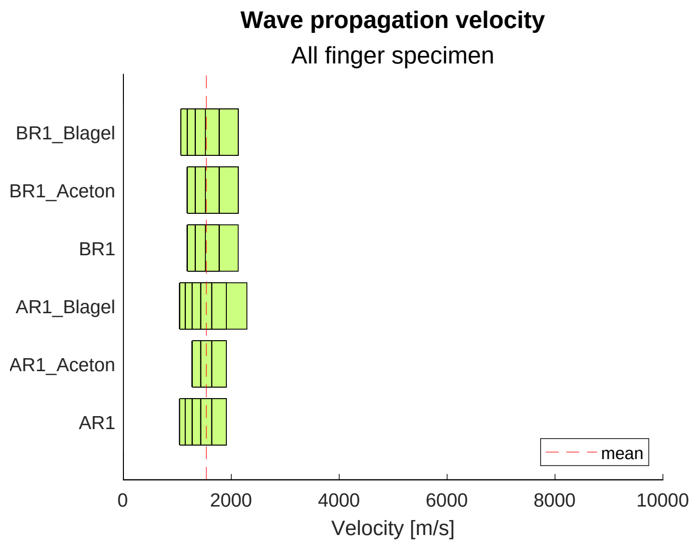

(a) All finger specimen

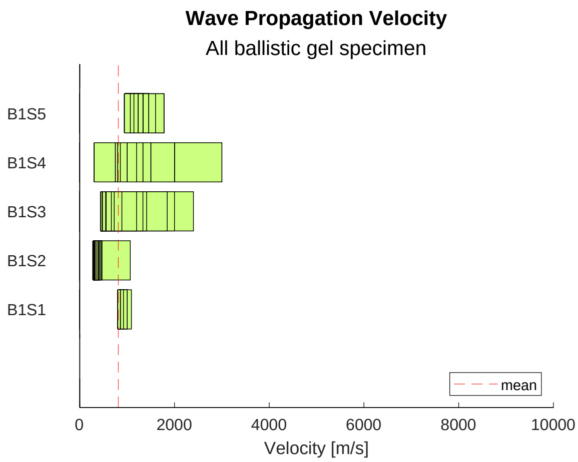

(b) All ballistic gel specimen

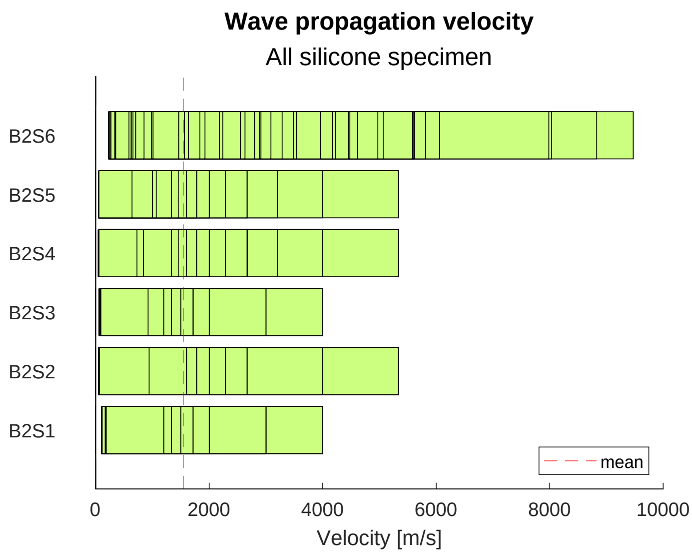

(c) All silicone specimen

Figure 3.5: The grouped specimen for the different types of specimen.

As can be seen in Figure 3.5a the measured wave propagation velocity varies from around 1000 m/s to over 2000 m/s. However, the variability between the different fingers with the exception of person A for electro-conductive gel treated finger is according to Levene's test not significantly different with a factor of significance at $\alpha = 0.05$. For person A the variability of untreated, acetone treated, and electro-conductive gel treated fingers are significantly different according to Levene's test. However to note is that the variance of untreated finger and acetone treated finger had a lower total variance and are not significantly different according to Levene's test. For person B the variance of untreated finger, acetone treated, and electro-conductive gel treated fingers are not significant different according to Levene's test.

In total there were 72 samples of mean wave propagation velocity were collected for each finger which in total gives 432 real finger samples. In Table 3.1 the number of samples measured for each finger specimen and the mean wave propagation measured for the fingers specimen can be seen. The mean of these gives a mean wave propagation velocity of around 1540 m/s.

In Figure 3.5b the mean wave propagation velocity measured for the ballistic gel specimen can be seen. The variations for each specimen are very different. It is not possible to perform a Levene's test to compare the variations because of the different number of data sets of samples collected for each specimen.

In Table 3.1 the number of samples collected for each specimen and mean wave propagation for all ballistic gel specimen can be seen. The mean average wave propagation velocity for all ballistic gel specimen is around 600 m/s.

In Figure 3.5b the mean wave propagation velocity measured for the silicone specimen can be seen. The variations for each specimen are high but similar to each other. The variations of all silicone specimen compared to each other are not significantly different from each other according to Levene's test.

In Table 3.1 the number of samples measured for each silicone specimen and the mean wave propagation for all silicone specimen can be seen. The mean wave propagation for all silicone specimen is around 1190 m/s.

In Figure 3.6 the distribution in form of a histogram over the wave propagation velocity measurements for the different types of specimen can be seen.

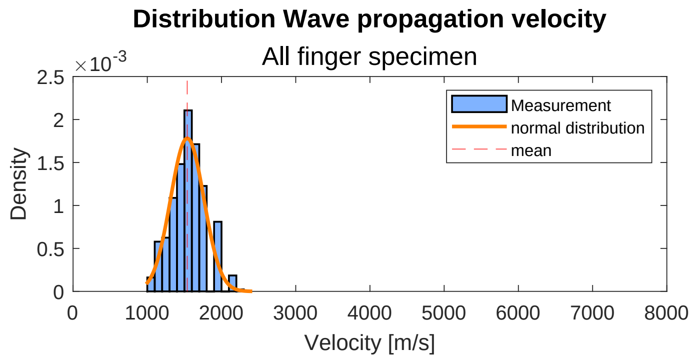

(a) All finger specimen

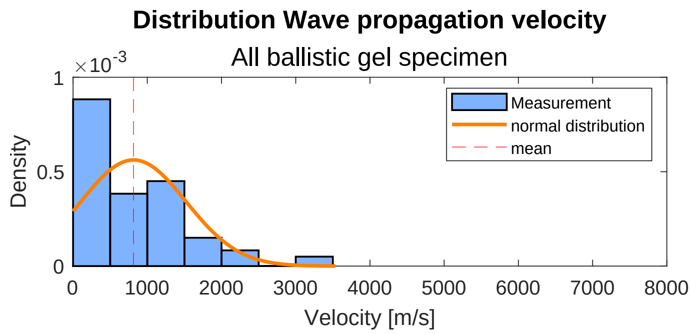

(b) All ballistic gel specimen

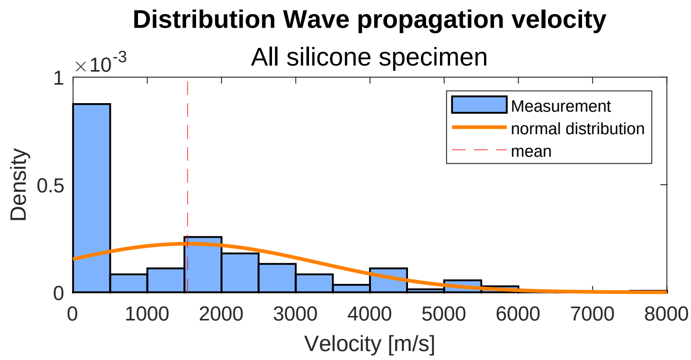

(c) All silicone specimen

Figure 3.6: Distribution of the wave propagation velocity measurements for the different types of specimen.

As can be seen in Figure 3.6a the distribution fingers specimen shows resemblance to the normal distribution. It should be noted that some velocity intervals have either very few or no measurement.

In Figure 3.6b the distribution of ballistic gel specimen can be seen. The distribution do not seem to follow a normal distribution. In this case there are many instances in the first interval and then similar number of instances for all following intervals.

In Figure 3.6c the distribution of silicone specimen can be seen. The distribution do not seem to follow a normal distribution either. In this case there are many instances in the first interval and then similar number of instances for all following intervals.

3.1.3 Max acceleration

The max acceleration for the experimentally gathered data was analysed. The analysis included a comparison of different load cases for the same specimen and between groups of specimens of the same type, such as fingers, ballistic gel and silicone molding compound. Furthermore, will the different types specimen be compared. Lastly will the difference between the type of treatment made on the finger surface, such as application of acetone and electro-conductive gel be compared.

The measured specimen results were combined into groups for each individual specimen and each individual loading case, independently of date the experiment were performed. Levene's test was then preformed for each specimen and its different loading cases.

First will the result of the finger specimen be considered. In Figure 3.7 the finger specimen is combined into groups for each individual loading case independently of date can be seen.

The variances between the loading cases for each individual specimen were all significantly different according to Levene's test. It was therefore not assumed that the data sets for each loading case could be combined into the group of responses for each specimen. However, it should be noted that all specimen have similar span for the different load cases. It could therefore be assumed that the load case has more influence on the max acceleration than different fingers and finger treatments.

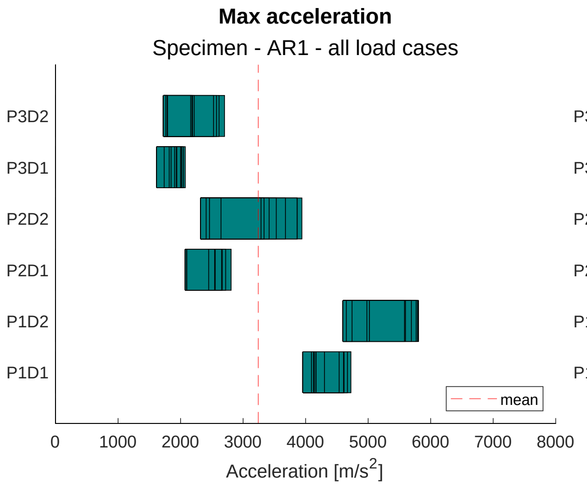

(a) Specimen $AR1$.

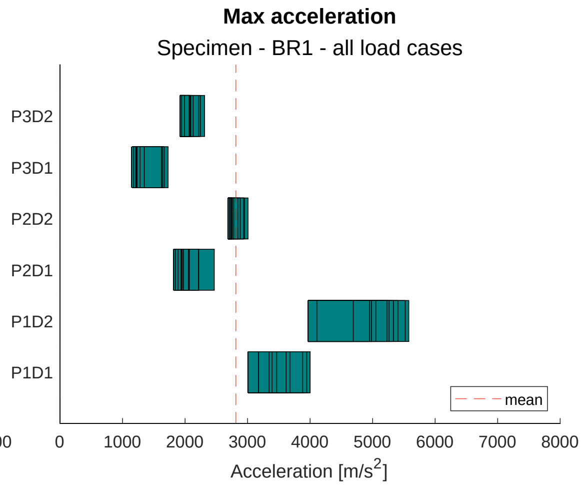

(b) Specimen $BR1$.

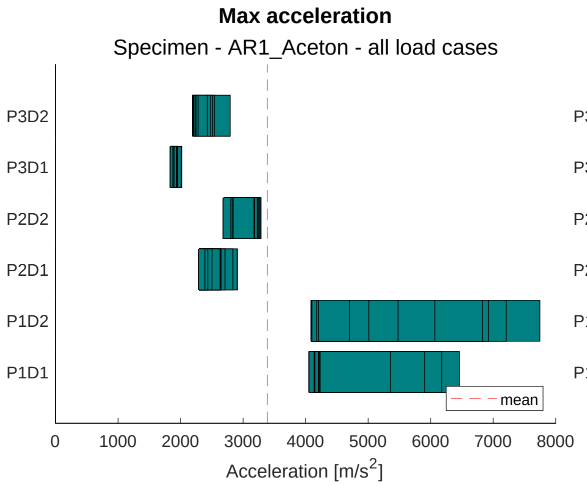

(c) Specimen $AR1\_Aceton$.

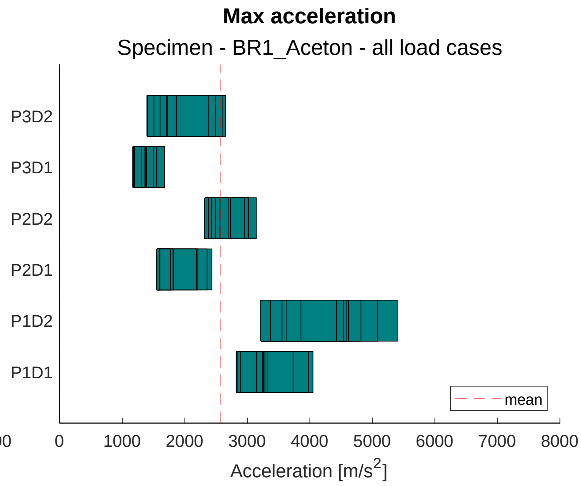

(d) Specimen $BR1\_Aceton$.

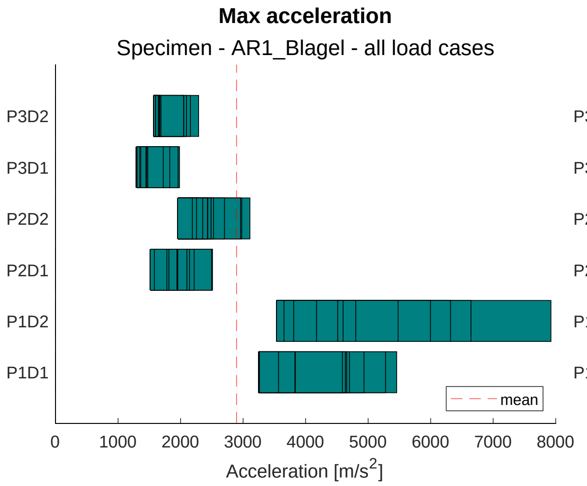

(e) Specimen $AR1\_Blagel$.

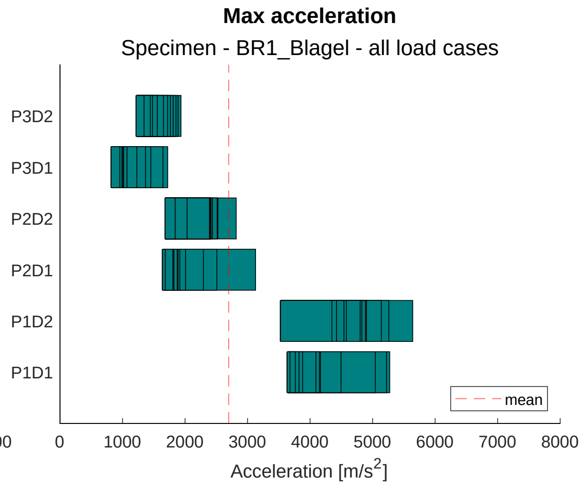

(f) Specimen $BR1\_Blagel$.

Figure 3.7: The max acceleration for each finger specimen combined into groups for each individual loading case independently of date. Individual measurement are represented by black lines in the span.

Next is the max acceleration for the ballistic gel specimen considered. In Figure 3.8 the ballistic gel specimen is combined into groups for each individual loading case independently of date can be seen.

According to Levene's test the variance of specimen $B1S2$ and $B1S4$ was not significantly different. The rest of the specimen had significantly different variances. Both specimen $B1S2$ and $B1S4$ had steel as substitute for bone. Specimen $B1S3$ which has a p-value at 0.04, close to the factor of significance, also had steel as substitute for bone. This could indicate that steel substitute gives a more consistent max acceleration than wood substitute.

In Figure 3.9 the max acceleration measured for the silicone specimen can be seen. The variances between load cases is not significantly different according to Levene's test with the exception of specimen $B2S4$. However, it should be noted that the span and variance of all the specimen are much higher than for the finger specimen. It can therefore be assumed that for silicone substitute fingers the max acceleration does not depend on the load case.

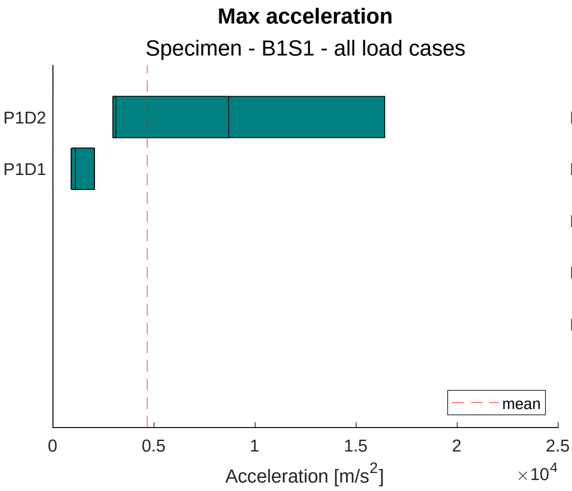

(a) Specimen $B1S1$.

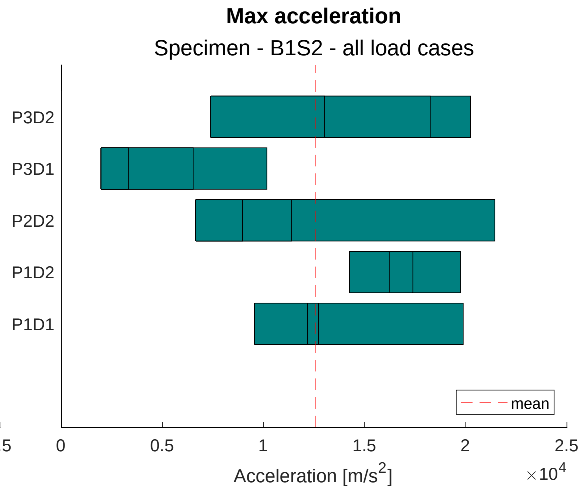

(b) Specimen $B1S2$.

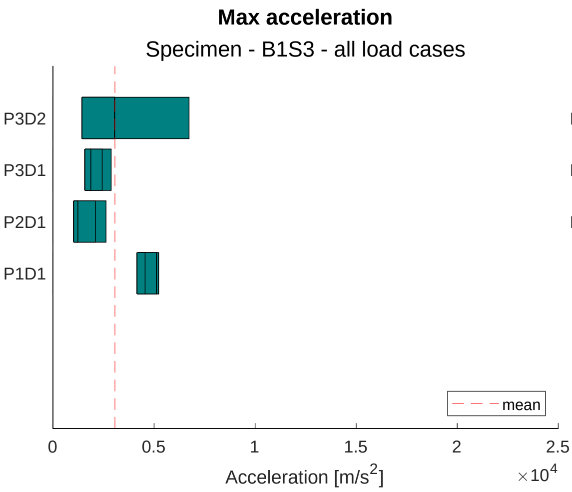

(c) Specimen $B1S3$.

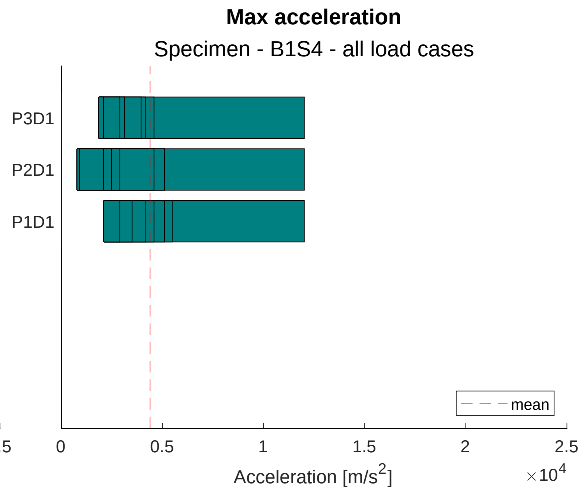

(d) Specimen $B1S4$.

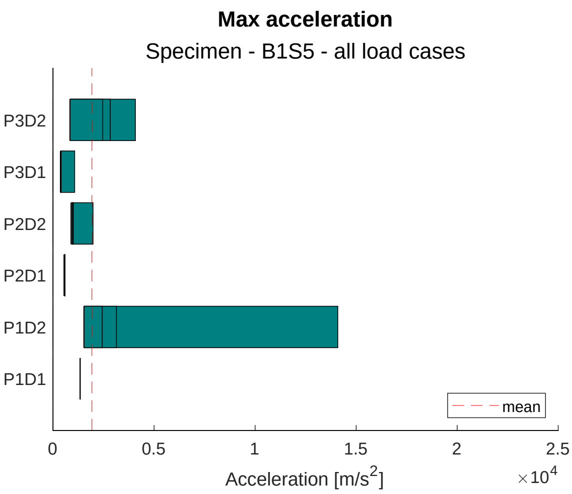

(e) Specimen $B1S5$.

Figure 3.8: The max acceleration for each ballistic gel specimen combined into groups for each individual loading case independently of date. Individual measurement are represented by black lines in the span.

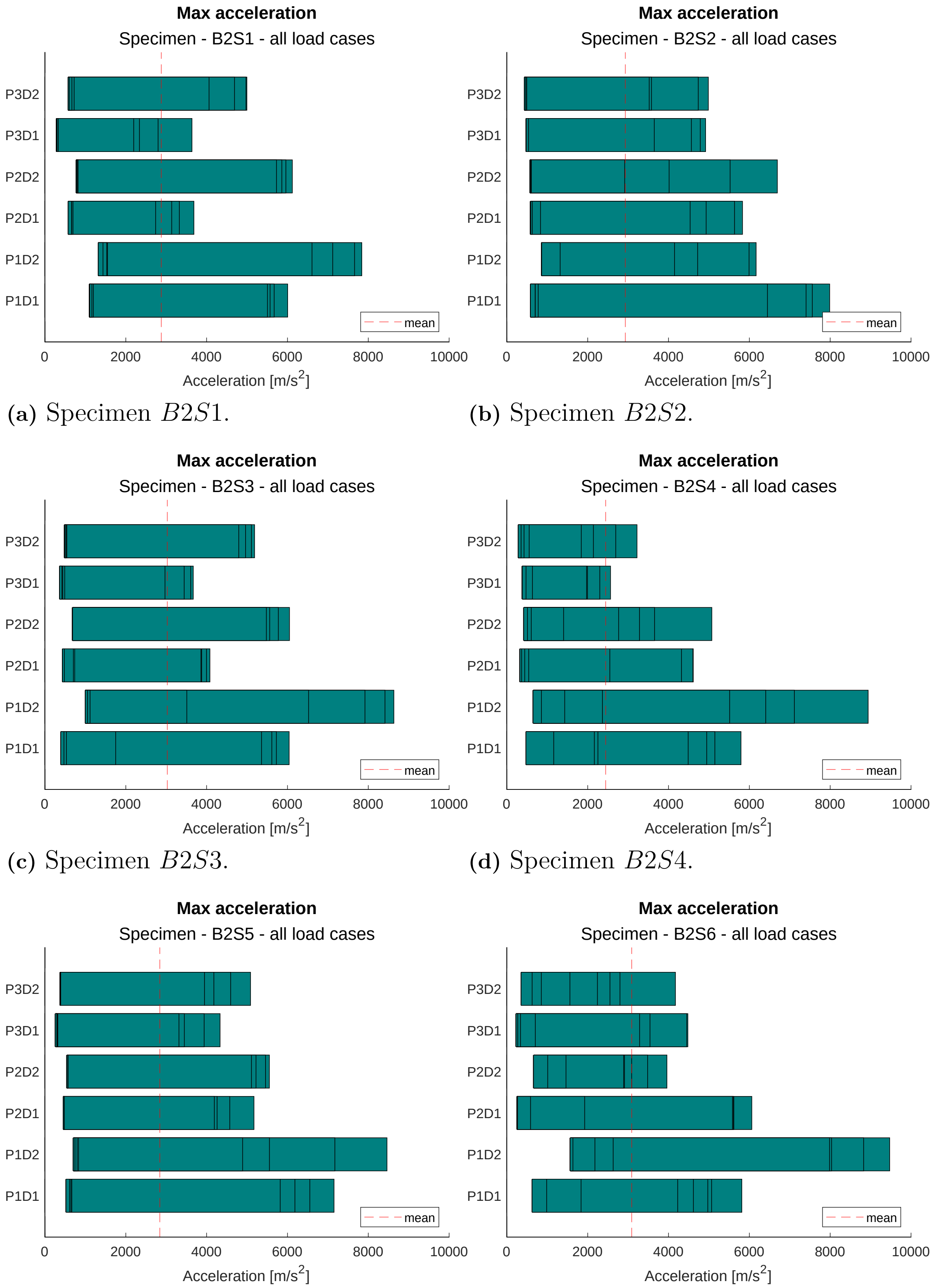

(a) Specimen $B2S1$.

(b) Specimen $B2S2$.

(c) Specimen $B2S3$.

(d) Specimen $B2S4$.

(e) Specimen $B2S5$.

(f) Specimen $B2S6$.

Figure 3.9: The max acceleration for each silicone specimen combined into groups for each individual loading case independently of date. Individual measurement are represented by black lines in the span.

It should be noted that for the finger specimen the max acceleration occurs at the start of the initial impulse. However for the ballistic gel specimen and silicone specimen the max acceleration often occurs later in the impulse. The max acceleration of the ballistic gel and silicone specimen could therefore have been influenced by reflections within the specimen.

In Table 3.2 the max acceleration and p-value for each specimen as well as the number of data sets of samples included in each specimen and total number of samples for the different types of specimen can be seen.

Specimen	**mean MA [m/s^2]**	**p-value**	**Number of samples**
AR1	3242	0.0002	72
AR1_Acetone	3387	0.0	72
AR1_Blagel	2895	0.0	72
BR1	2813	0.0	72
BR1_Acetone	2565	0.0002	72
BR1_Blagel	2698	0.02	72
B1S1	4659	0.004	8
B1S2	12556	0.55	20
B1S3	3064	0.04	16
B1S4	4387	0.9	24
B1S5	1919	0.0	24
B2S1	2878	0.21	48
B2S2	2931	0.72	48
B2S3	3027	0.41	48
B2S4	2444	0.04	48
B2S5	2842	0.69	48
B2S6	3089	0.05	48

Table 3.2: Max acceleration and p-value for each specimen as well as the number of data sets of samples included in each specimen and total number of samples for the different types of specimen. MA denotes max acceleration.

3.2 FE model

Here the results from the 1D FE model is presented. The first part looks into what role dimension and position of the bone have to the wave propagation velocity and the dynamic response. The second part shows the reflection behaviour of a mechanical wave in terms of choice of material parameters of the bone. It also shows how the response of the nail is varying in combination with reflections within the structure. The third part accounts for the convergence study. Finally the results from a real input to the 1D FE model is examined and compared.

3.2.1 Geometry and dimension

When comparing the result in Figure 3.10 the real and the homogeneous geometry FE models show no similarities in the dynamic response with the exception of the input curve. Table 3.3 shows the time it took for the wave to reach each node for the two models. The time for node 4 shows the largest difference and the other nodes show little difference in terms of wave propagation velocity between the two tested models.

Node#	1	2	3	4
Time (homogeneous column) [μs]	0	1.994	4.994	10.99
Time (real column) [μs]	0	2.0	5.0	7.99

Table 3.3: Dynamic response of the two FE models. In the zoomed in view of Figure 3.10 the time of wave arrival can be seen.

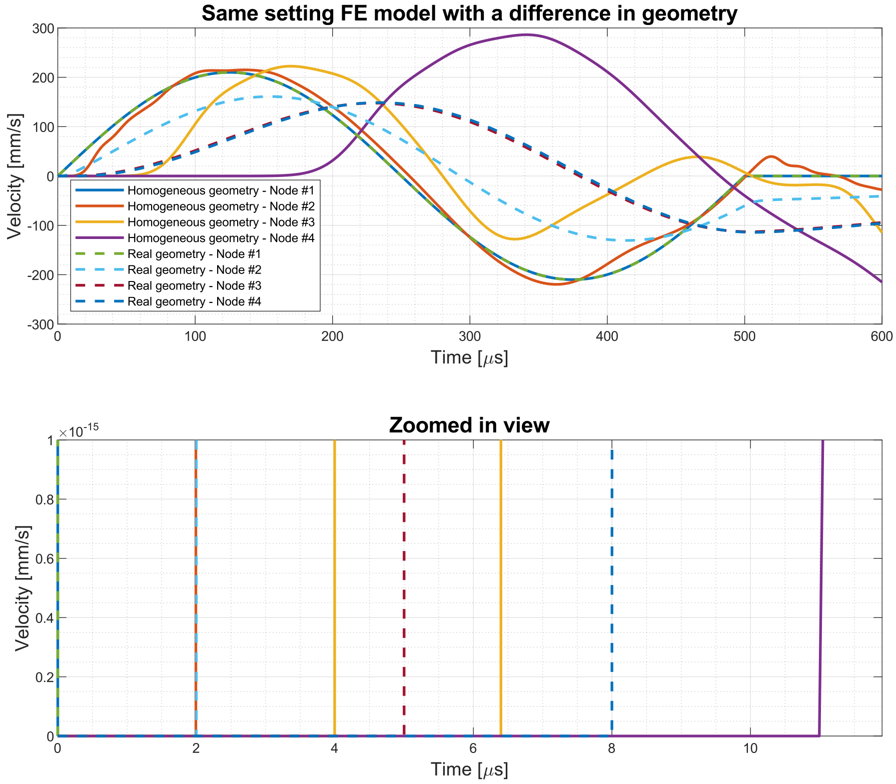

Figure 3.10: The solid lines are the homogeneous column and the dashed lines are the real thicknesses of the constituent layers. Note that the input for both scenarios is overlapping. It is evident that the dynamics within the finger depends on how the geometry is setup.

3.2.2 Wave reflection

The phenomenon of a mechanical wave reflection at the boundary between two materials was observed. For this section consider Figure 3.11 where it shows how the reflection depends both on the bulk modulus and the density. A comparison between the values of reflection and the displacement at the nail shows that the magnitude of reflection inside the structure at node #2 have influence on the magnitude of the displacement at the nail. The influence is that a reduced magnitude of displacement at the nail gives a greater magnitude of reflection inside the structure and vice versa. Furthermore, for the reflection and the dynamic response at the nail for bulk K_1 it is noted that a large-magnitude reflection gives a lesser response at the nail in terms of displacement, which applies to all tested material settings, see Tables 3.6 and 3.7 for a comparative study. In the considered figures it is clear that a greater value of reflection lowers the displacement at the nail. The largest value of reflection was observed for ρ_2 and K_2 which indicate that the reflective wave is positively interfered, meaning that the combination of material parameters causes resonance. Consider the plots for ρ_1-reflection and K_1-reflection and study the case for the nail response at a fixed density, ρ_1, the bulk modulus needs to have a large value to give a reflective response. Whilst changing the density for a fixed bulk modulus, K_1 gave a larger reflective response. Comparing the reflection and the dynamic response for bulk K_1 it was noted that a larger reflection gives a lesser dynamic response in terms of displacement at the nail. For the different material settings studied in this particular case it is apparent that a relatively high value of reflection lowers the displacement at the nail and this phenomenon can be viewed in all the plots of Figure 3.11.

It could be observed that the density and the bulk modulus of the bone also affected the dynamic characteristics and velocity of the wave that propagated through the 1D model. It was noted that the time it took for the wave to propagate through the 1D model was faster for the case of homogeneous density, ρ_1, compared to the higher values of density, see Table 3.4. This is likely due to the propagating wave is not reflected in its movement through the 1D model. The opposite is observed for an increase in density and bulk modulus where interference of waves is more prominent. As expected both the density and the bulk modulus affect the wave propagation velocity. According to Equation 2.3, the fastest wave propagation velocity is expected to be for the configuration K_1 and ρ_3, see Table 3.5. But evidently this has the slowest total wave propagation velocity, see Table 3.4. The fastest wave propagation is found when the material parameters of the bone equal are set to ρ_1 and K_2.

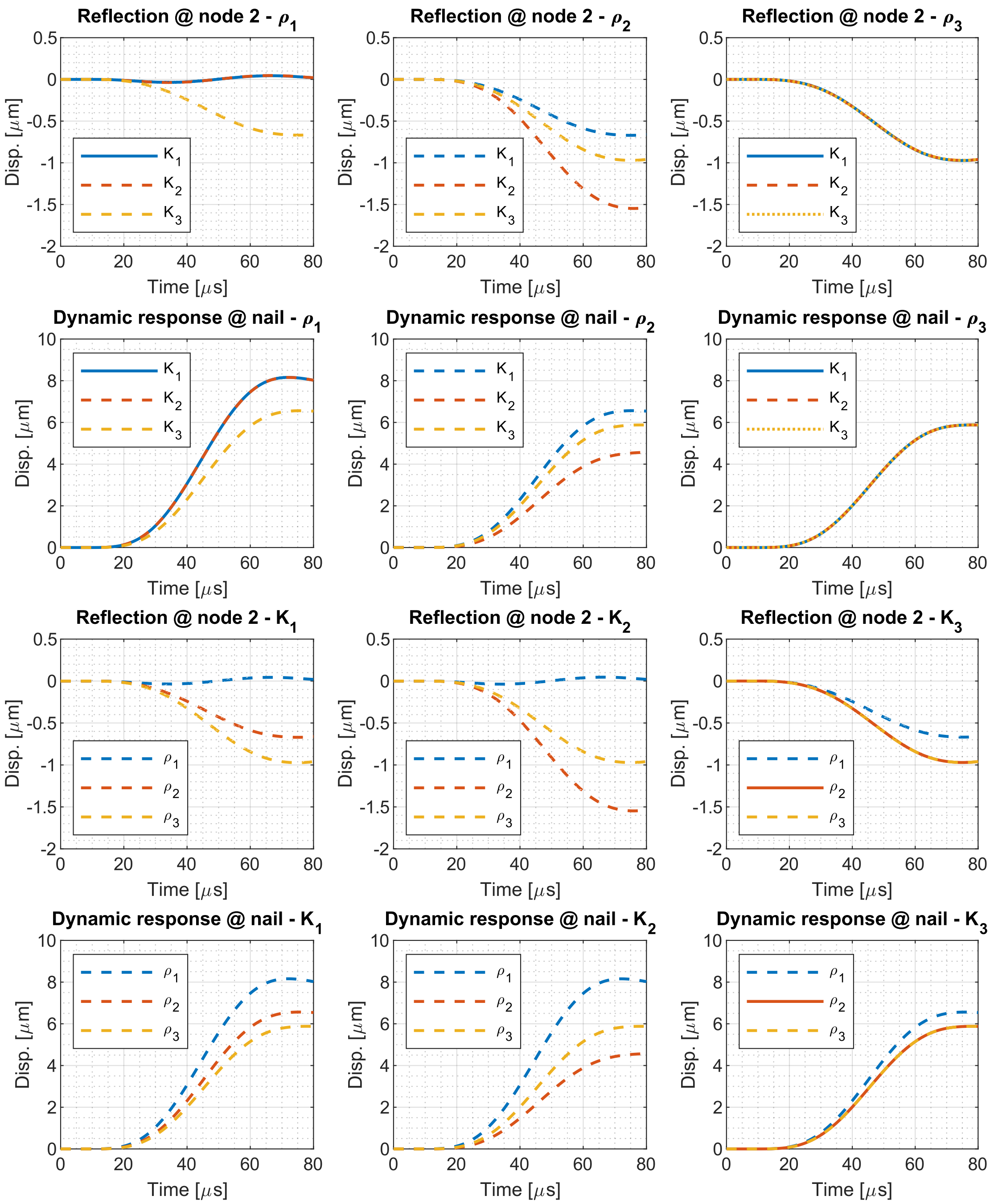

Figure 3.11: Time in microseconds on the abscissa and displacement in micrometers on the ordinate axis.

Nail response[μs]	K_1	K_2	K_3
ρ_1	7.545	7.233	7.263
ρ_2	7.824	7.78	7.348
ρ_3	7.965	7.54	7.348

Table 3.4: Time table of when the wave reached the nail.

In theory fastest velocity[-]	K_1	K_2	K_3
ρ_1	0.577	0.456	0.412
ρ_2	0.816	0.645	0.583
ρ_3	1.00	0.790	0.714

Table 3.5: Normalized wave propagation velocity where the expected fastest wave propagation velocity should occur. Normalization has been made with the fastest velocity.

Reflection[μm]	K_1	K_2	K_3
ρ_1	0.044	0.044	-0.6598
ρ_2	-0.6628	-1.519	-0.9579
ρ_3	-0.960	-0.9588	-0.9580

Table 3.6: Reflection of node #2 at 70 μs.

Nail displacement[μm]	K_1	K_2	K_3
ρ_1	8.143	8.143	6.496
ρ_2	6.5	4.43	5.786
ρ_3	5.786	5.786	5.786

Table 3.7: Displacement of the nail at 70 μs.

3.2.3 Mesh convergence

The mesh convergence study shows that the previously used combination of material parameters (remember that the mesh convergence used, as the only exception, the material parameters most recently used in the 2D-model) have a wave propagation velocity around 1900 [m/s]. This is within the span of the measurements and above the mean wave propagation velocity.

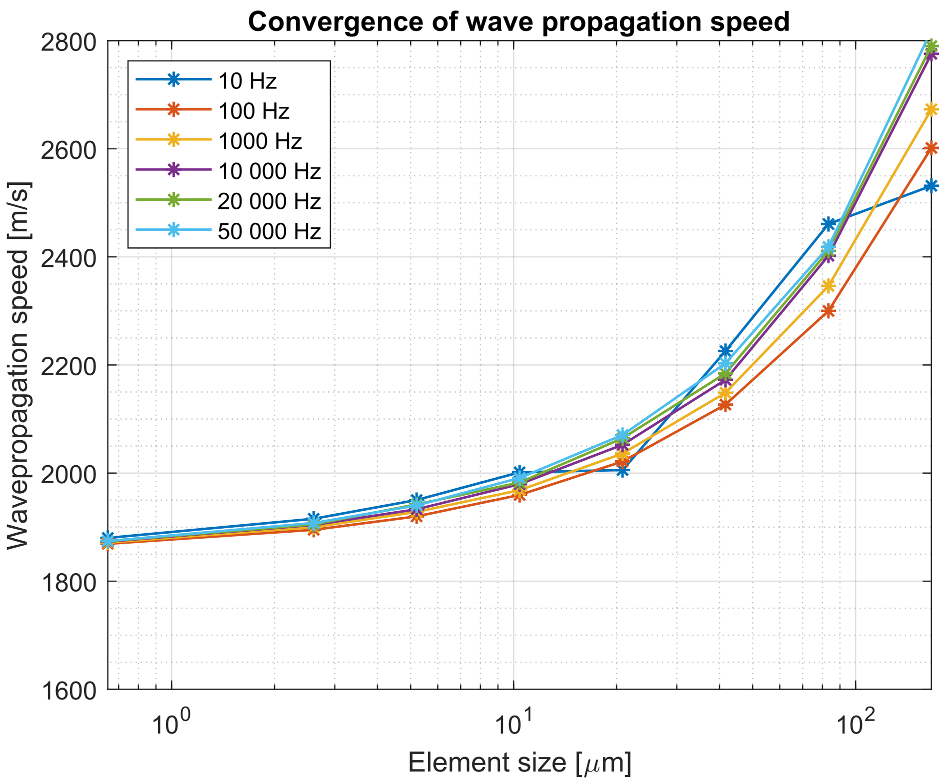

Figure 3.12: Convergence study of a real scale 1D column. For more details of the actual mesh size see Figure A.2 in Appendix

3.2.4 Real response

In Figures 3.13 and 3.14 it is shown how the material parameters affect to the output curve. For a fixed value of density the bulk modulus does not affect the output significantly. It is clear that the density affects the dynamic behaviour more than the bulk modulus when considering the applied damping cases.

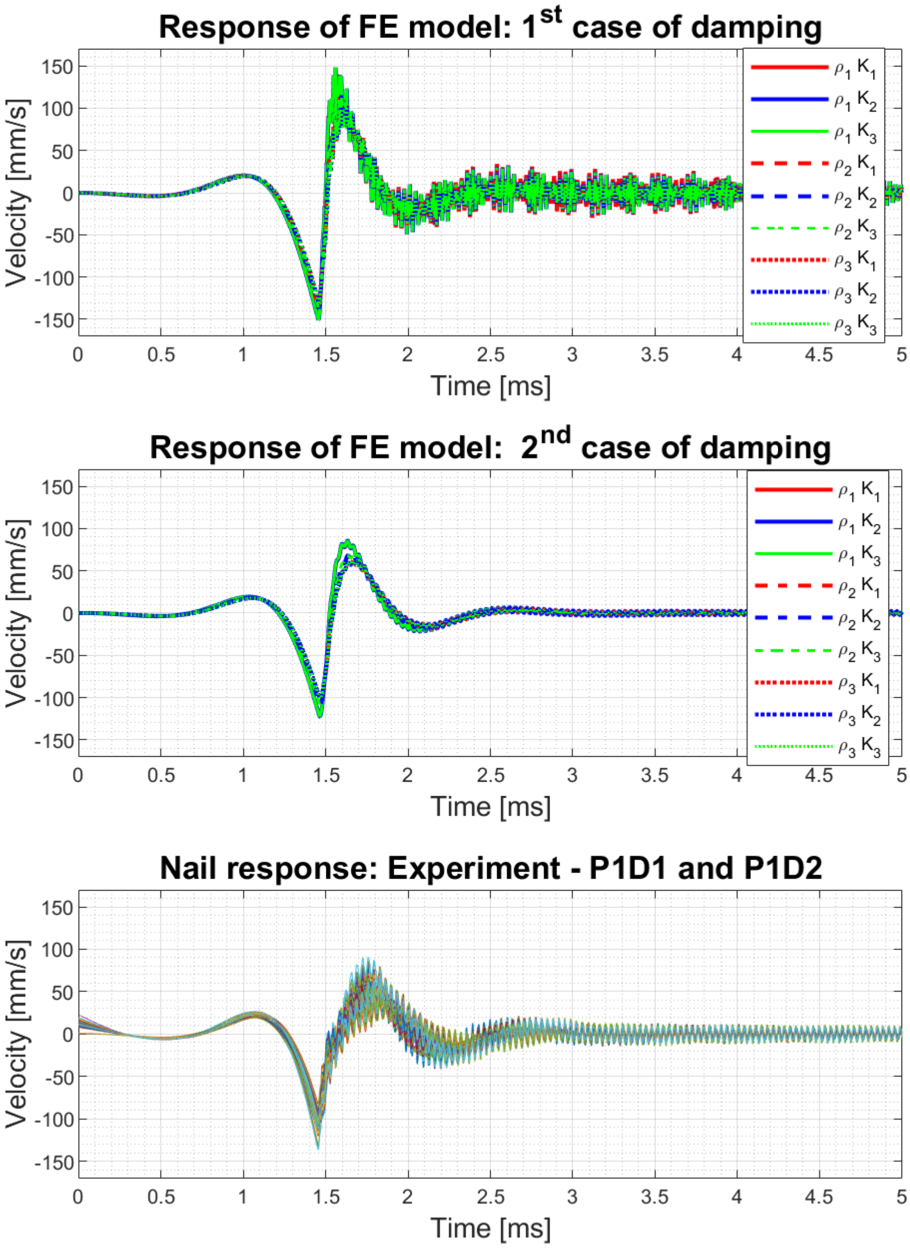

Figure 3.13: Here are the outputs of two cases of damping and the experimental output from P1D1 and P1D2 load cases. The FE model input correspond to the P1D1 cylinder input.

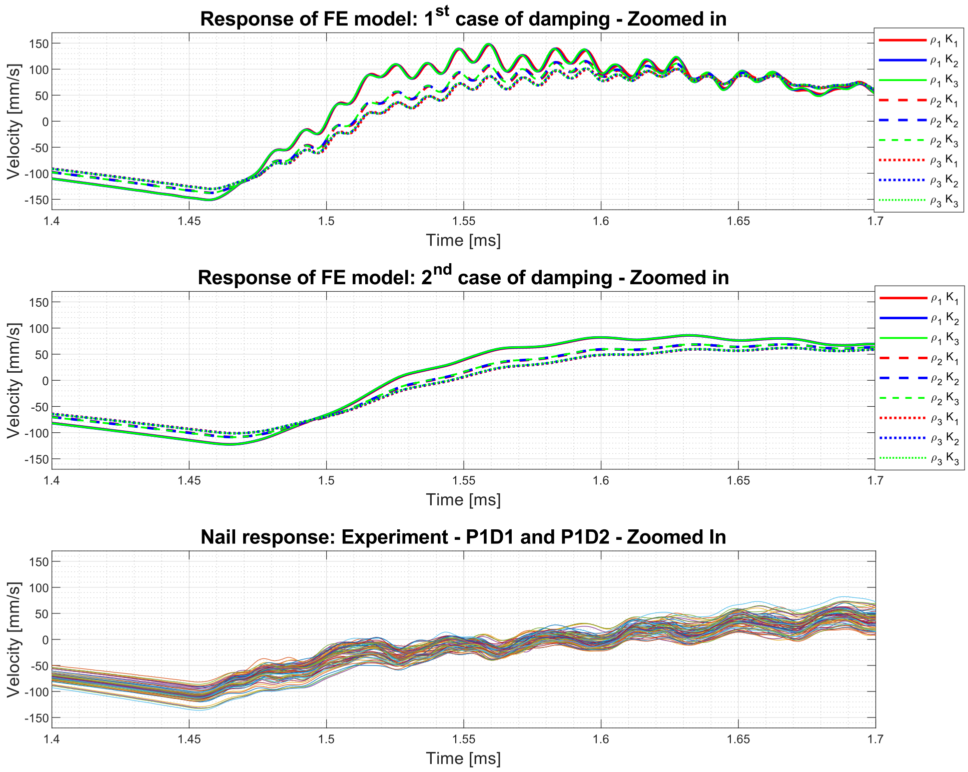

Figure 3.14: Zoomed in view of Figure 3.13. Effect of bulk modulus, density and added constant damping to parts of the structure.

Consider Figure 3.15 where the frequency spectrum for the input and output signals from experiments and from the two cases of damping is presented. Comparing the input to the FE model one notes that the overall characteristics are preserved but with a slightly reduced amplitude for the lower frequencies and a more significant reduction for the frequencies around 28 500 Hz. Considering the nail response from experiments there is a similar damping for the frequencies around 28 500 Hz but there is a significant difference in character for the lower frequencies. This can also be seen in Figure 3.13 where the shape of the real output between 1.5 - 2 ms resembles that of a pure sinusoidal wave. Compare this to the FE output in the same time span where the shape is much steeper and sharper.

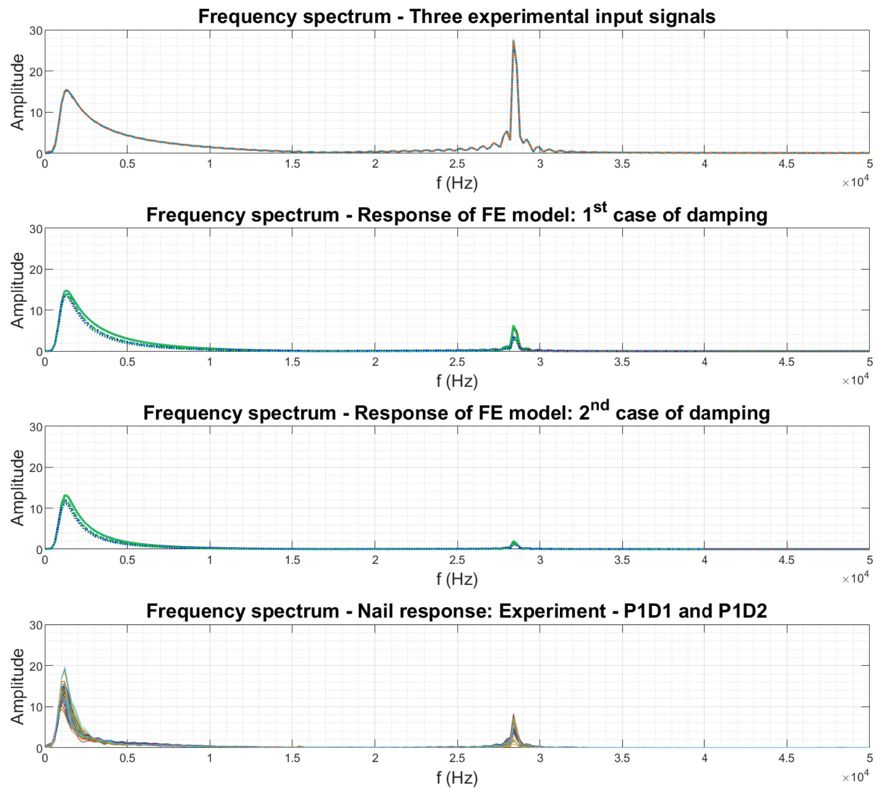

Figure 3.15: Frequency spectrum from experiment input/output and from FE model for two different settings of damping. The two curves in the middle both have the frequency response from all nine combinations of bulk modulus and density.

In Figure 3.16 a zoomed in view of the high frequency content is compared. Here it can be seen that the first and second cases of damping and the experimental curves show a similar reduction of amplitude. The maximum peak value of the first case of damping and the minimum peak value of the second case of damping can be seen as two black horizontal lines in the zoomed in frequency spectrum for the nail response in Figure 3.16. For the dominant 28 500 Hz frequency the damping of the finger and the FE model are similar In Figure 3.17 the results from the FE show characteristics that is more similar to the input curve than the actual frequency response from the finger. The experimental spectrum shows a faster decline after 1200 Hz compared to the input and FE spectrum. There is a clear difference in the characteristics between the FE and the experimental part.

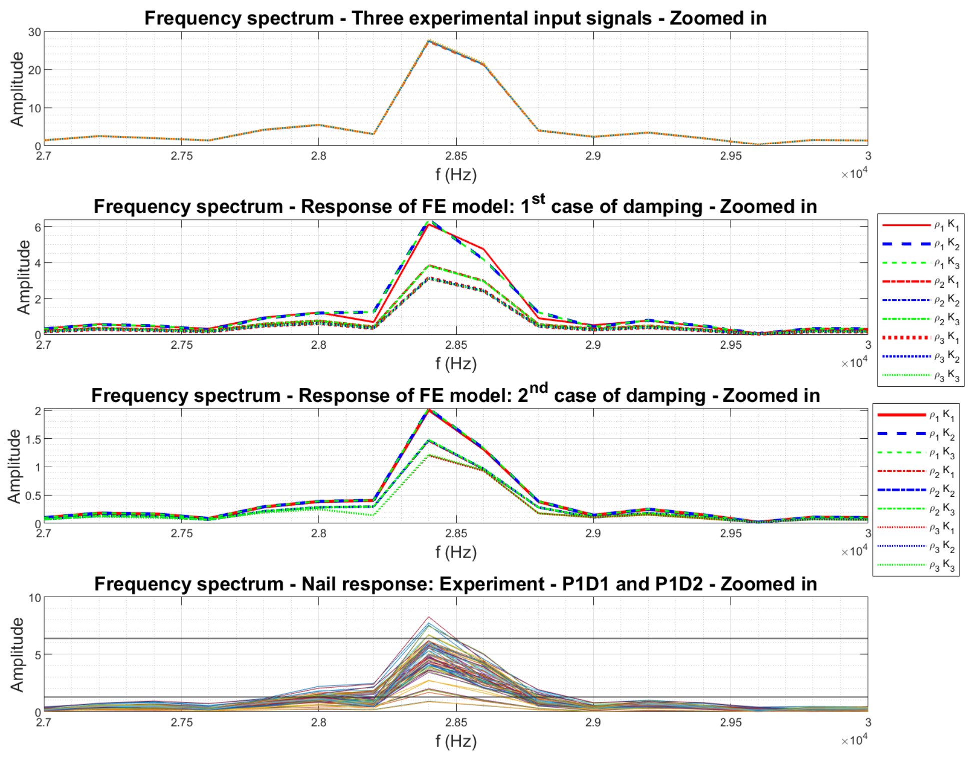

Figure 3.16: Zoomed in view of how the bulk modulus and density affect the frequency spectrum. A lower peak is a higher density value.

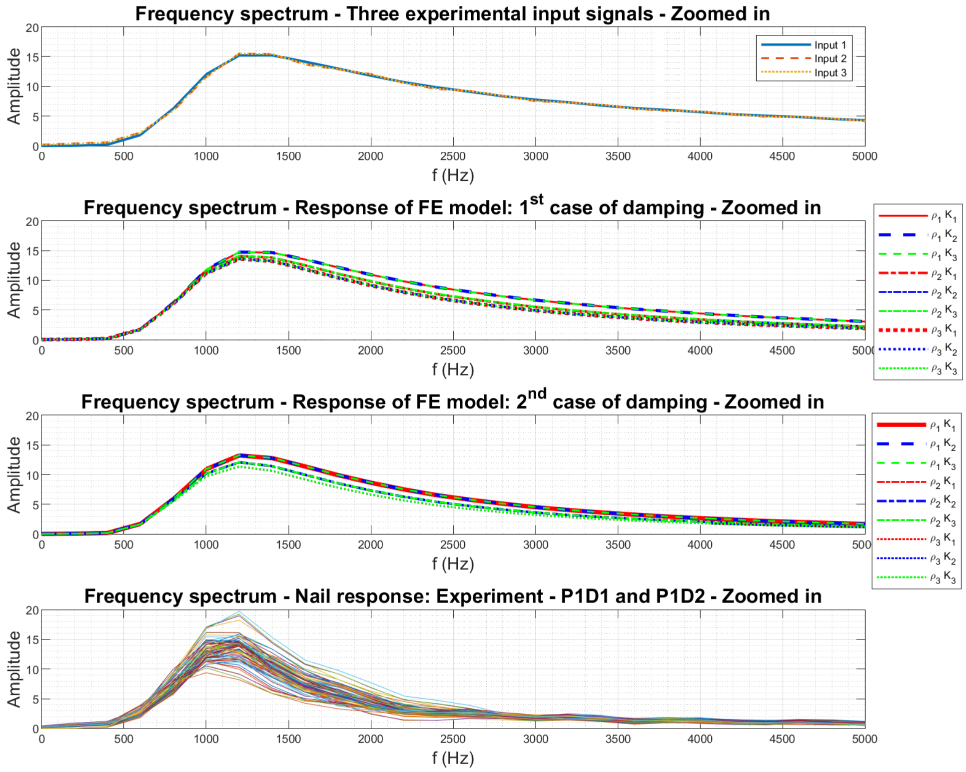

Figure 3.17: Zoomed in view of the lower frequency part of the spectrum. Here 0 – 5000 Hz is shown.

4 Discussion

First the experiments of the finger substitutes is discussed followed by a more extensive discussion on the FE modelling and results.

4.1 Experiments - Substitute fingers

As has been previously described it was difficult to repeat the testing multiple times for the ballistic gel specimen due to it breaking apart from either the load or natural degradation. Most specimen were therefore only tested during one day, which included just a few experiments for each loading case, and the maximum number of experiments lasted for two days for some specimen. Some specimen did not sustain even one test for the higher pressure and others could preform all load cases for two dates before natural degradation made the specimen unfit for testing. The bone-like segment of the specimen was of the same dimension for all samples. The load distribution area internally remains the same between the bone and tissue when applying pressure. However, different specimen with the same tissue dimension survived for different amount of pressure and time. The only specimen surviving for all pressures and more than one date was specimen $B1S5$. The fact that this specimen was able to sustain the testing over time could be a result of that wood substitute was more elastic than steel when applying pressure. It could also be a result of that steel has a larger heat conductivity than wood. The specimen with steel as substitute material to bone could get much colder in storage. This could have made the ballistic gel more brittle and crack easier when pressure was applied. The specimen $B1S1$ had wood as substitute to bone but smaller tissue dimension which could possibly be too small for the load and therefore the tissue cracked.

The limited number of samples combined with the different total number of samples for different specimen could question the assumption of combining the different loading cases into one response variation for each specimen. However, this should give the ballistic gel specimen an advantage in getting a smaller span and lower variation of wave propagation velocities. But in Figure 3.5 it can be seen that the majority of ballistic gel specimen have either a larger span or similar in size to finger specimens. This means that even if the ballistic gel specimens had a larger advantage of becoming more consistent the majority of the specimen were more inconsistent than finger specimens.

It should however be noted that the specimen $B1S5$ has a wave propagation velocity variation that is very similar to the finger variations. Also, the span of measurements for specimen $B1S5$ is overlapping the spans of measurements for most of the real finger specimen. If wave propagation velocity is considered, specimen $B1S5$ could work as a substitute for fingers. However, the overall dynamic response of the $B1S5$ specimen is not comparable to real fingers.

In Figure 3.1 the ballistic specimen has no visible dominant dynamic response between the measurements. The method used to derive wave propagation velocity could therefore become more arbitrary than for the finger specimen. It is not as clear, for the ballistic gel specimen, where the initial impulse starts because of more varying amplitude, phase shifted signals and high amplitude noise in the response. Therefore the time increment of initial response could not be determined automatically at the lowest point. The time increment were therefore to be derived manually for the ballistic gel specimen which is less accurate. Even small differences in time increment could lead to a large difference in the resulting calculated wave propagation velocity.

The silicon specimen were not made of bio-material and henceforth did not have the same problem of natural degradation as the ballistic gel specimen. Furthermore, the silicon specimen did not break due to the applied pressure during the experiment. The same number of experiments could therefore be performed for all silicon specimen. The silicon specimen seem superior to ballistic gel specimen considering the physical behaviour at test, i.e. does not crack. Furthermore it can be seen in Figure 3.1 that the dynamic response of the silicon specimen is more similar to the fingers with a dominant lower frequency and higher frequency oscillations. However, the response had higher phase shift between different measurements than the fingers had.

The wave propagation velocity variation for all silicon specimen independent of the bone substitute is much higher than for fingers and ballistic gel specimen. Furthermore, it is easier to track the initial impulse for the silicon specimen than for the ballistic gel specimen because of the more dominant lower frequency response. The measurement of the time increments for the initial pulse should therefore be more accurate and on par with the finger measurement.

In this study the date has not been considered as a factor due to limitations. It should however be noted that specifically for the silicon specimen there were a notable difference in phase shift for different dates. The silicon specimen could therefore be much more prone to factors related to temperature, moisture in the air or possible hardening of the silicon. Therefore, the silicon specimen could potentially be more accurate if these factors were considered. But as a test of the repeatability over time the silicon specimen does not preform better or even close to the real finger measurement.

4.2 FE - Geometry

In the aspect of wave dynamics within the model and at the surface of the 1D FE model, geometry and position of the constituent layers of the FE model affects the dynamic response. For the wave propagation velocity it is not that clear. Looking at nodes 2 and 3 in Figure 2.3 there is little difference in terms of wave propagation velocity and this small difference is likely due to short distances and similar material properties in terms of density and bulk modulus. However, the visible difference is probably due to differences in how the stress is characterized as a product of the layer thicknesses which again suggests that the geometry has significant affect not only on the propagating wave but also how the displacement field will be characterized. The nodes from where measurement were taken have the same coordinates, but they do not sit in the same material as can be seen in Figure 2.3. This could explain the slight difference in time since node 3 sits in the denser bone material for the homogeneous model. However it does not explain the faster time for node 2 which, again, points to the stress characteristic argument. To explain the fastest total time however; the real geometry possesses the largest portion of dense bone which speed up the total wave propagation velocity as can be seen in Table 3.3. As can be seen in Figure 3.10 it is evident that the dynamics are very different when contrasting the two models.

4.3 FE - Wave reflection

The wave reflections and the nail responses show both similarities and variation for the varying material parameters of the bone. Variations of the dynamic response at the nail, for all the material parameters studied, reveal that the amplitude of the reflecting wave vary inside the finger. Additionally, the conditions inside the finger and between tissues and ligaments determine how the wave will propagate through the structure. The difference in density (previously seen in the results) between two adjacent materials determines these characteristics regarding the reflections and transmissions from the incident waves that stems from the vibrating source (the cylinder). It is this difference in density between materials and Newtons third law that determine the size and sign of the wave amplitude that are reflected and transmitted through the structure [18]. For example, assume a structure initially at rest, then a wave is generated and it travels through a less dense medium towards a more dense medium. When the wave reached the more dense medium the reflected part of the wave will be inverted (change sign), which is due to the heavier material overpowers (Newtons third law) the lighter material at the boundary. The transmitted wave, is the part of the wave that is not being reflected, will not be inverted but will be affected by the interaction from the less dense medium. The former described reflective phenomenon can be seen in Figure 3.11 where the reflection waves shows a negative value for the cases where the bone had a larger density.

4.4 FE - Boundary and initial conditions

The application of the load at the boundary might cause problems in terms of introducing unwanted tension stresses that could have an impact on the outcome of the simulation. However, for this study this was assumed to be negligible.

Considering the FE modelling, the static force compensation is important to reproduce the load scenario of the experiment properly. However, a pre-loaded phase was not used in this work for the 1D FE model.

The static force compensation was also made to show, in the event of a reproduction of the experiment, that the force measured by the dynamometer was in practice less than the amount recorded and used in this work. However, this force was small and deemed negligible in the experiment. With that stated, the experiment setup would benefit to have the hammer disconnected to the rig. This would remove the influence of the hammer completely, which would render the experiment somewhat more consistent.

4.5 FE - Real input

The results showed that it is possible to get somewhat similar output from the FE model compared to the experimental output. There is a difference in damping between the real finger and the FE model. This is something that was expected. However, it is interesting to note that from a relatively crude damping implementation done by trial and error methods in LS-DYNA it is possible to reach similar in characteristics.

The input used in the FE model was from the loading case P1D1. This input curve was produced with an applied force of 4 N to the cylinder, note that these 4 N has not been statically compensated as mentioned in Section 2.2.2. This is not the case for the 1D FE model, i.e. the structure was not in a stress state when the load was applied.

4.6 FE - Mesh convergence

The approach of the mesh convergence has been discussed several times between the authors. Since wave propagation velocity was the quantity that was used to check convergence there might be an issue of answering the question of what quality of mesh that is needed in order to capture a certain frequency. The wave propagation velocity shows that in order to get a convergent result the mesh needs to be very fine regardless of the frequency of the input. However, this tells us that in order to capture the correct wave propagation it is necessary to have a very fine mesh regardless of frequency. In this work it is assumed that the high frequency content of the real input (thus, also the output) was captured properly since an element size based on the convergence study made was used. In Figure 4.1 it can be seen how the curves converges towards the 7.5 microsecond mark, the increase in steepness of the curve "take off" indicate that it requires higher frequencies to enable such a sharp turn. Additionally, the frequency spectra shown in Figure 3.15 strengthen our assumption that a sufficient mesh was used.

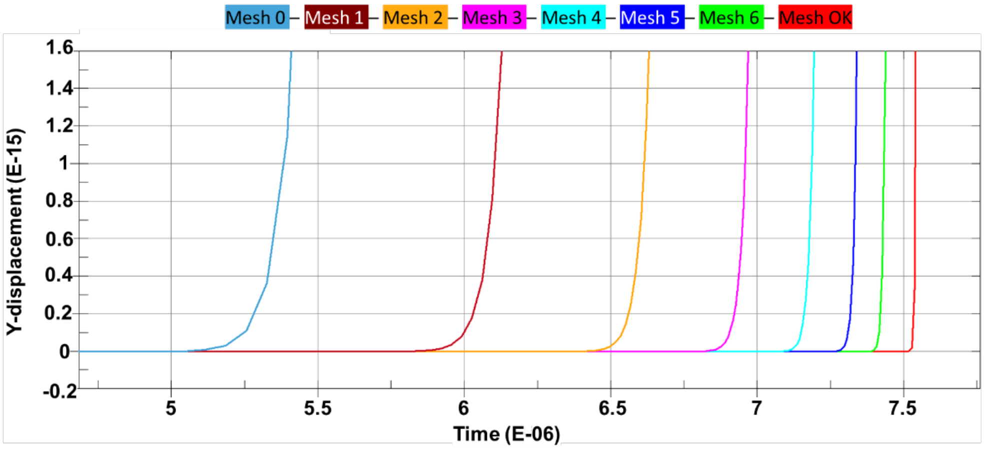

Figure 4.1: The curves show the different mesh sizes and the convergence towards 7.5 microseconds. Where the light blue 'Mesh 0' to the far left corresponds to the coarsest mesh and 'Mesh OK' corresponds to the finest mesh quality.

5
Conclusion

The dynamic response measured on the nail of the fingers were very similar between all finger specimen independent of person, date or load case. There is no noticeable difference between the untreated and treated fingers, were the treatment amplified the two extremes of present or lack of fingerprint. The mean wave propagation velocity variance between untreated and treated fingers were not significantly different to each other in a general sense. The conclusion is therefore that the finger print does not influence the resulting dynamic response or the wave propagating through the finger at all or it is not large enough to be measured by the experiment set-up. However the experiments are unable to measure local effects in the finger near the tool and fingerprints. The effects in dynamic response and wave propagation velocity inside the finger can therefore still be affected by fingerprints.

The dynamic response of the ballistic gel substitute specimen were noticeable different to the dynamic response of the fingers. Furthermore, the dynamic responses were less consistent between different load cases and dates than for the fingers. The mean wave propagation velocity were more varied than for fingers specimen with exception of specimen with more elastic bone substitute. The distribution of the wave propagation velocity measurements were different as well. The finger specimen measurements seemed to follow a normal distribution but the ballistic gel specimen did not. Multiple of the ballistic gel specimen had catastrophic failure and cracked. Furthermore, the specimen suffered natural degradation rendering it not reliable for consistent measurements over time . With this in consideration it can be concluded that a substitute finger made of ballistic gel is not a viable alternative to derive accurate experimental data to represent real fingers.

The dynamic response of silicone substitute specimen were more similar to the dynamic response of the fingers than the ballistic gel specimen. However the silicone dynamic response was still noticeable different compared to the fingers. The silicone specimen are also less consistent between different load cases and dates. The variation of the wave propagation velocities were much larger for the silicone specimen than finger specimen. The distribution of measurements for the silicone specimen seems to not follow a normal distribution. With this in consideration it can be concluded that substitute fingers made of silicone in the form tested in this study is not a viable alternative to derive accurate experimental data to represent real fingers.

The conclusions of the geometry study is that the dimension and position of the synthesizing layers in the geometry of the 1D FE models affect the dynamic response and the wave propagation velocity, both internally and externally. Therefore, to properly design a future FE-model care needs to be taken when choosing the finger cross section geometry and dimensions to better match experimental data.

It is shown that by trial-and-error methods of implementing damping to the 1D FE models that it is possible to improve the FE output such that its characteristics resemble the experimental output. The two damping cases show that in order to capture the characteristics of the experimental output curve properly a more sophisticated damping scheme needs to be applied.

Based on the 1D FE model the dynamic response (reflection and transmission at material interfaces) inside the finger can significantly differ depending on the material parameters chosen. Still the response at the nail in terms of maximum velocity is still within the allowed interval from the experiments, which is true for the two applied cases of damping. This means that the variations that was seen of the possible reflections inside the geometry as a function of the material parameters are all plausible as long as the nail-response, for the same material parameters, stay within the experimental velocity maximum peak value interval. With regard to this the current details inside the 2D model is a viable solution.

Experimental data show that the maximum velocity value for all experimental load cases for the real finger can be found in the interval 20-150 [mm/s] and the FE results from the same input gave a max velocity peak value interval of 50-150 [mm/s] for all bulk modulus and density values considered. Additionally, the frequency spectrum for the same FE model shows that the FE curve for the first case of damping have the same higher end frequency content and amplitude as the equivalent experimental frequency spectrum. However, the lower portion of the frequency spectrum is not the same and the FE frequency spectrum for the first case of damping contains more frequencies than the equivalent experimental spectrum. This leads to the conclusion that at the present moment the FE model lacks the ability to damp some of the frequencies when compared the experiment frequency spectrum. This means that the 1D FE model contains more waves than what is seen in the experiment. Thus, analysing any stresses and strains from the FE model is likely to be over-estimated since the majority of the wave has not been dissipated in the structure.

6
Recommendations for future work

In this chapter suggestions and advice for future studies will be discussed.

For future studies on human finger subjected to shock vibration loading it would be relevant to preform more experiments of real fingers to derive even more accurate data of the dynamic response of fingers depending on different factors. This should include a large number of different individuals, several load cases and could even include additional factors such as temperature and moisture to further the understanding of the dynamic response of fingers.

When the hammer strikes the cylinder and generate the impulse to the cylinder the boundary condition between the finger and the tool is presumed such that there is no gap allowed between the cylinder surface and the skin of the finger in contact. Assuming that this boundary condition holds the following aspects are good subjects of study to replicate the conditions in a FE environment.

If the boundary condition is set to fix the boundary between the finger and the tool then the gap will always be zero, i.e in practice gluing the finger to the tool in the model. However this will maintain a zero gap as a consequence of that the tool will drag back the finger. This will affect the strain and strain rate of the finger at least locally near the contact. This boundary condition could represent a real phenomenon if for example a negative pressure is established between the finger and tool. If this boundary condition is set and strain and strain rate is studied it must be verified that the finger is not leaving the cylinder due to, for example negative pressure or some other phenomenon that produces the same boundary condition.

If the boundary condition is to be maintained by a large enough prescribed force to the finger to compensate for the force of the impulse from the tool then the gap between the finger and the tool could remain zero. The impulse is however in some cases up towards 10 000 m/s^2 in magnitude which results in a large impulse force. Therefore to fulfill the condition of no gap the prescribed force must be equally as large. In testing of this boundary condition with provided material data and the force applied to the bone has this resulted in the bone tearing through the tissue by the prescribed force. It could be studied with a varying reaction force to compensate for the impulse force but not maintain a large static force on or in the finger. However the realism of a such force could be argued. It should also be noted that even for these large forces it could be seen that for some nodes there was gap when the impulse was applied. There could therefore be some numerical errors in calculation and set up of the contact in the FE model. One alternative to solve this could be that even if a very small gap is present it can be considered as still being in contact. Furthermore if some part of the finger is experiencing gap but not the entire finger, this could possibly still be considered as in contact. Previous studies [10] has concluded that the finger is in contact with the tool for the entire impulse, however it could be studied on a smaller scale what contact means more precisely, i.e. is there some allowable gap between finger and surface in terms of the FE-model?

If the boundary condition is to be maintained by fixing some nodes from either the bone, nail or tissue in space to limit the movement could the gap between the finger and the tool could remain zero. However this have showed to have the same problem of some individual nodes in contact experience gap. Furthermore this will influence the strain in the model. Possibly could the end of the nail have a prescribed motion represented by experimental measured data. This will have the same effect as the negative pressure of the finger being dragged introducing unrealistic strains in the finger. However in this case the largest effect of this will be near the nail and not the contact between the finger and tool. Therefore this could possibly give more accurate result near the contact which is the area of most interest when studying damage to the fingers.

With the provided 2D FE model the finger is already deformed by the prescribed pressure. This was done due to eliminate the need for large deformation of the model because when the prescribed load was applied the deformation were much smaller. However this also eliminates the strain derived by the prescribed load. A undeformed 2D model could therefore be used to give more accurate strain in the model. The large difference in deformation could be solved by dynamic relaxation were the large deformation is applied as a static load while the fast impulse is applied as a dynamic load. When tested the dynamic relaxation approach has had the same problem as just applying a prescribed force as a boundary condition in that the gap will occur. This could however be combined by locking nodes in space after the static load is applied but before the dynamic impulse load is applied.

The geometry and dimensions of the 2D FE model could be reconsidered because it has been shown that the geometry and dimensions influence the response of the model. In Figure 6.1a an undeformed 2D FE model with more realistic dimensions, bone geometry and nail placement can be seen.

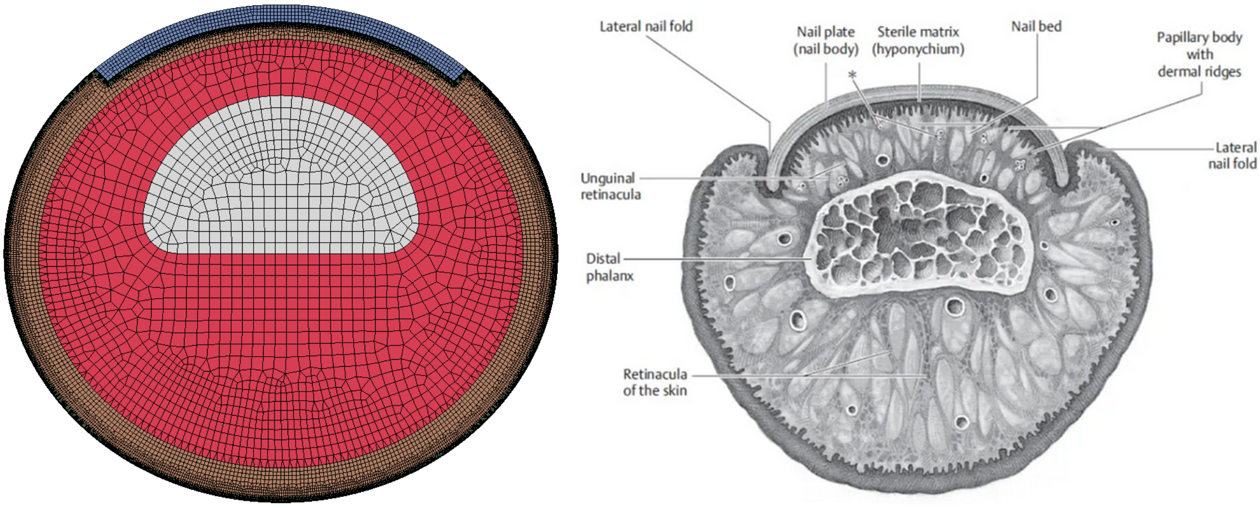

(a) Suggestion of 2D FE model based on cross section in (**b**).

(b) Cross section of finger tip anatomy [21].

Figure 6.1: Suggestion of how to improve the current 2D FE model. The bone can be even further approved by the 'honey comb'-like structure seen in (b).

The stress and strain field could be compared for the boundary condition of a prescribed velocity input directly onto the nodes and for a case where the nail is locked in a FE environment. This would possibly reveal the extent of the tension stresses that the current prescribed velocity might introduce.

Lastly, determine the correct damping coefficients through a 1D model to properly capture the dissipative forces in order to close the gap between FE and experiment. If the 1D FE output could be matched and properly compared with the experimental data and perhaps a 1D analytical model could be derived. This would be a great starting position to vary the parameters such that the output curve is always met but the dynamic response inside the finger vary.

References

[1] Swedish Work Enviroment Authority. *Statistik om vibrationer.* https://www.av.se/halsa-och-sakerhet/vibrationer/statistik-om-vibrationer/. [Online; accessed: 2022-01-25].

[2] Svenska institutet för standarder. *SVENSK STANDARD SS-EN ISO 5349-1:Vibration och stöt – Mätning och bedömning av vibrationer som överförs till handen – Del 1: Allmänna riktlinjer (ISO 5349-1:2001)*, chapter Annex A. Svenska institutet för standarder, 2001-09-07.

[3] Hans Lindell. *Attenuation of hand-held machine vibrations: Application of non-linear tuned vibration absorbers*. Lic. Thesis, Chalmers University of Technology, 2017.

[4] European Agency for Safety and Health at Work. *Directive 2002/44/EC - vibration.* https://osha.europa.eu/sv/legislation/directives/19. [Online; accessed: 2022-05-30].

[5] RISE. *Most common occupational injury preventable.* https://www.ri.se/sv/berattelser/most-common-occupational-injury-preventable. [Online; accessed: 2022-02-04].

[6] AFA Försäkring. *Ny rapport pekar ut verktygen som orsakar vibrationsskador.* https://www.afaforsakring.se/nyhetsrum/pressmeddelanden/2018/09/ny-rapport-pekar-ut-verktygen-som-orsakar-vibrationsskador/. [Online; accessed: 2022-05-30].

[7] Wilfredo Lopez-Ojeda; Amarendra Pandey; Mandy Alhajj; Amanda M. Oakley. *Anatomy, Skin (Integument).* https://www.ncbi.nlm.nih.gov/books/NBK441980/. [Online; accessed: 2022-06-02].

[8] Karolinska Institutet. *Epidermis.* https://mesh.kib.ki.se/term/D004817/epidermis. [Online; accessed: 2022-06-30].

[9] Vildsvinsbutiken. *Ballistic Gel-till Handladdaren.* https://vildsvin.se/handladdning/ovrigt/ballistic-gel-till-handladdaren/. [Online; accessed: 2022-06-17].

[10] Jesper Lennartsson Oskar Malm Emelie Svensson Marcus Alverstrand, Elin Dufvenius Esping. Ultravibrationer i mänskliga fingrar och hur fingrar förhåller sig till en vibrerande yta: Kandidatarbete inom mekanik och maritima vetenskaper. Chalmers University of Technology, 2021.

[11] MathWorks. *vartestn: Multiple-sample tests for equal variances.* https://se.mathworks.com/help/stats/vartestn.html. [Online; accessed: 2022-05-10].

[12] Livermore Software Technology. *About LS-PrePost.* https://www.lstc.com/products/ls-prepost. [Online; accessed: 2022-06-01].

[13] Livermore Software Technology. *LS-DYNA Manual Volume I R13*. https://www.dynasupport.com/manuals/ls-dyna-manuals/ls-dyna_manual_volume_i_r13.pdf. [Online; accessed: 2022-06-04].

[14] Livermore Software Technology. *LS-DYNA manual Vol II R6.1.0*. https://ftp.lstc.com/anonymous/outgoing/jday/manuals/LS-DYNA_manual_Vol_II_R6.1.0.pdf. [Online; accessed: 2022-06-02].

[15] Galli F. Incrocci L. Smijs T. Hosseinzoi, A. Mechanical Properties of Healthy and ex vivo Onychomycosis Nails and the Influence of a Porphyrin-propylene Glycol Antifungal Formulation. *Current Journal of Applied Science and Technology*, 14:1–14, 2016.

[16] Matthias Graw Steffen Peldschus Zahra Asgharpour, Peter Zioupos. Development of a strain rate dependent material model of human cortical bone for computer-aided reconstruction of injury mechanisms. *Forensic Science International*, 236:109–116, 2014.

[17] Anna Yarusskaya. *Density of Bone*. https://hypertextbook.com/facts/2002/AnnaYarusskaya.shtml. [Online; accessed: 2022-06-01].

[18] Physics Classroom. *Boundary Behavior*. https://www.physicsclassroom.com/class/waves/Lesson-3/Boundary-Behavior. [Online; accessed: 2022-06-02].

[19] Livermore Software Technology. *Damping*. https://www.dynasupport.com/howtos/general/damping. [Online; accessed: 2022-06-02].

[20] Bertil Thomas. *Modern Reglerteknik*. Liber, 2016.

[21] Reuben A. Bueno Nada N. Berry and Elvin Zook. *The Nail and Finger Pulp*. https://musculoskeletalkey.com/37-the-nail-and-finger-pulp/. [Online; accessed: 2022-06-01].

A

Appendix

A.1 Static compensation in test setup

In this section the derivation of static compensation for the finger force can be seen.

In Figure A.1 the hammer components can be seen. Force components F_{Oy} and F_{Ox} are the reaction force in the rotation point O and the force F_{mg} is the gravity acting on the hammer. The mass of the hammer is $m = 0.12$kg and the gravity acceleration is assumed to be $g = 9.81\ m/s^2$. Before release, the hammer rests on a finger at the release angle theta. Neglecting friction, the reaction on the hammer is described by the external force F_f. A radius, r, describes the length of the arm from rotation point O to the force F_f. The length l is the length of the arm from rotation point O and center of mass of the hammer. The angle θ comes from the position of the hammer.

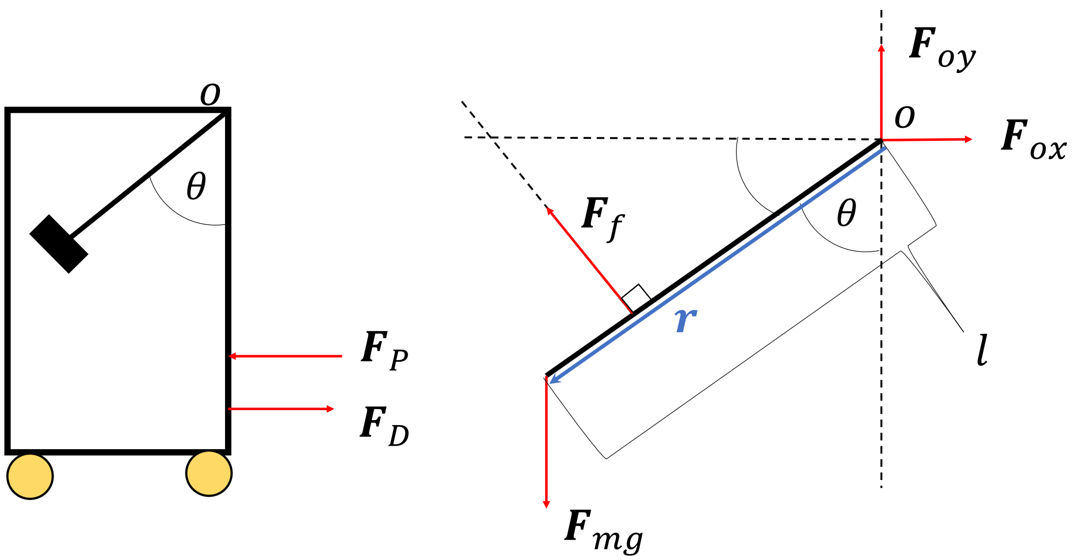

Figure A.1: Forces acting on the rig and hammer.

The force components:

The horizontal forces

$$\begin{aligned} &F_{Ox} - \cos(\theta)\ F_f = 0 \\ &=>\ \ F_{Ox} = \cos(\theta)\ F_f. \end{aligned} \tag{A.1}$$

The moment in point O

$$\begin{aligned} &mgl - sin(\theta)F_f r = 0 \\ &=>\ \ F_f = \frac{mgl}{sin(\theta)r}. \end{aligned} \tag{A.2}$$

If the force F_f is acting in the center of mass of the hammer, i.e $r = l$ can this be rewritten as

$$F_f = \frac{mg}{sin(\theta)}. \tag{A.3}$$

Combined horizontal force component in point O is given by

$$F_{Ox} = \frac{cos(\theta)}{sin(\theta)} mg. \tag{A.4}$$

The actual force of the finger, F_p is then given by the force measured by the dynamometer subtracted by the horizontal reaction force. I.e

$$F_P = F_D - F_{Ox}. \tag{A.5}$$

A.2 Table of mesh convergence

Real scale model - 10 Hz	Mesh 0	Mesh 1	Mesh 2	Mesh 3	Mesh 4	Mesh 5	Mesh 6	Mesh Overkill
Length [mm]	14.1	14.1	14.1	14.1	14.1	14.1	14.1	14.1
Time between first input/output [ms].	5.57E-03	5.73E-03	6.34E-03	7.03E-03	7.05E-03	7.23E-03	7.36E-03	7.50E-03
Wave Prop. Speed [m/s]	2.53E+03	2460.733	2225.73007	2005.69	2001.419	1950.207469	1915.500611	1880.050135
Difference in between meshes	70.68532809	235.00291	220.040171	4.270454	51.21198	34.70685755	35.45047666	0
INFO								
Smallest mesh size [mm]	0.1666	0.0833	0.04165	0.020825	0.010413	0.00520625	0.002603125	0.000650781
Smallest timestep	7.01E-08	3.50E-08	1.75E-08	8.76E-09	4.38E-09	2.19E-09	1.09E-09	2.73E-10
ASCII output frequency	10 Mhz	10 Mhz	10 Mhz	10 Mhz	10 Mhz	10 Mhz	10 Mhz	10 Mhz
Number of elements	54	108	162	216	270	324	378	432
Real scale model - 100 Hz	Mesh 0	Mesh 1	Mesh 2	Mesh 3	Mesh 4	Mesh 5	Mesh 6	Mesh Overkill
Length [mm]	14.1	14.1	14.1	14.1	14.1	14.1	14.1	14.1
Time between first input/output [ms].	5.42E-03	6.14E-03	6.63E-03	6.98E-03	7.20E-03	7.34E-03	7.44E-03	7.54E-03
Wave Prop. Speed [m/s]	2601.476015	2.30E+03	2126.69683	2021.505	1959.558	1919.934641	1895.110346	1869.183657
Difference in between meshes	305.0590766	169.72011	105.191456	61.94732	39.62342	24.82429403	25.92668926	0
INFO								
Smallest mesh size [mm]	0.1666	0.0833	0.04165	0.020825	0.010413	0.00520625	0.002603125	0.000650781
Smallest timestep	7.01E-08	3.50E-08	1.75E-08	8.76E-09	4.38E-09	2.19E-09	1.09E-09	2.73E-10
ASCII output frequency	10 Mhz	10 Mhz	10 Mhz	10 Mhz	10 Mhz	10 Mhz	10 Mhz	10 Mhz
Number of elements	54	108	162	216	270	324	378	432
Real scale model - 1000 Hz	Mesh 0	Mesh 1	Mesh 2	Mesh 3	Mesh 4	Mesh 5	Mesh 6	Mesh Overkill
Length [mm]	14.1	14.1	14.1	14.1	14.1	14.1	14.1	14.1
Time between first input/output [ms].	5.28E-03	6.01E-03	6.56E-03	6.93E-03	7.16E-03	7.31E-03	7.42E-03	7.53E-03
Wave Prop. Speed [m/s]	2672.985782	2346.0899	2148.57143	2036.101	1968.449	1928.205128	1900.013475	1871.515795
Difference in between meshes	326.8959317	197.51842	112.470346	67.65211	40.24385	28.19165293	28.49768021	0
INFO								
Smallest mesh size [mm]	0.1666	0.0833	0.04165	0.020825	0.010413	0.00520625	0.002603125	0.000650781
Smallest timestep	7.01E-08	3.50E-08	1.75E-08	8.76E-09	4.38E-09	2.19E-09	1.09E-09	2.73E-10
ASCII output frequency	10 Mhz	10 Mhz	10 Mhz	10 Mhz	10 Mhz	10 Mhz	10 Mhz	10 Mhz
Number of elements	54	108	162	216	270	324	378	432
Real scale model - 10000 Hz	Mesh 0	Mesh 1	Mesh 2	Mesh 3	Mesh 4	Mesh 5	Mesh 6	Mesh Overkill
Length [mm]	14.1	14.1	14.1	14.1	14.1	14.1	14.1	14.1
Time between first input/output [ms].	5.08E-03	5.87E-03	6.49E-03	6.87E-03	7.12E-03	7.29E-03	7.41E-03	7.53E-03
Wave Prop. Speed [m/s]	2775.590551	2402.0443	2172.57319	2052.402	1979.503	1933.095695	1904.118839	1873.256277
Difference in between meshes	373.5462582	229.4711	120.171443	72.89873	46.40732	28.97685647	30.86256122	0
INFO								
Smallest mesh size [mm]	0.1666	0.0833	0.04165	0.020825	0.010413	0.00520625	0.002603125	0.000650781
Smallest timestep	7.01E-08	3.50E-08	1.75E-08	8.76E-09	4.38E-09	2.19E-09	1.09E-09	2.73E-10
ASCII output frequency	10 Mhz	10 Mhz	10 Mhz	10 Mhz	10 Mhz	10 Mhz	10 Mhz	10 Mhz
Number of elements	54	108	162	216	270	324	378	432
Real scale model - 20000 Hz	Mesh 0	Mesh 1	Mesh 2	Mesh 3	Mesh 4	Mesh 5	Mesh 6	Mesh Overkill
Length [mm]	14.1	14.1	14.1	14.1	14.1	14.1	14.1	14.1
Time between first input/output [ms].	5.06E-03	5.85E-03	6.46E-03	6.83E-03	7.11E-03	7.26E-03	7.40E-03	7.52E-03
Wave Prop. Speed [m/s]	2.79E+03	2411.0807	2184.35321	2064.422	1982.565	1942.14876	1905.147953	1874.00319
Difference in between meshes	375.4805535	226.7275	119.931545	81.85699	40.41592	37.00080735	31.14476319	0
INFO								
Smallest mesh size [mm]	0.1666	0.0833	0.04165	0.020825	0.010413	0.00520625	0.002603125	0.000650781
Smallest timestep	7.01E-08	3.50E-08	1.75E-08	8.76E-09	4.38E-09	2.19E-09	1.09E-09	2.73E-10
ASCII output frequency	10 Mhz	10 Mhz	10 Mhz	10 Mhz	10 Mhz	10 Mhz	10 Mhz	10 Mhz
Number of elements	54	108	162	216	270	324	378	432
Real scale model - 50000 Hz	Mesh 0	Mesh 1	Mesh 2	Mesh 3	Mesh 4	Mesh 5	Mesh 6	Mesh Overkill
Length [mm]	14.1	14.1	14.1	14.1	14.1	14.1	14.1	14.1
Time between first input/output [ms].	5.00E-03	5.83E-03	6.40E-03	6.81E-03	7.08E-03	7.27E-03	7.39E-03	7.52E-03
Wave Prop. Speed [m/s]	2818.872451	2418.5249	2203.125	2070.485	1990.963	1940.144479	1907.725612	1874.376869
Difference in between meshes	400.3475797	215.39987	132.640419	79.52158	50.81853	32.41886661	33.34874284	0
INFO								
Smallest mesh size [mm]	0.1666	0.0833	0.04165	0.020825	0.010413	0.00520625	0.002603125	0.000650781
Smallest timestep	7.01E-08	3.50E-08	1.75E-08	8.76E-09	4.38E-09	2.19E-09	1.09E-09	2.73E-10
ASCII output frequency	10 Mhz	10 Mhz	10 Mhz	10 Mhz	10 Mhz	10 Mhz	10 Mhz	10 Mhz
Number of elements	54	108	162	216	270	324	378	432

Figure A.2: Table of mesh convergence study.

DEPARTMENT OF SOME SUBJECT OR TECHNOLOGY
CHALMERS UNIVERSITY OF TECHNOLOGY
Gothenburg, Sweden
www.chalmers.se

AVANCEZ 1829

CHALMERS
UNIVERSITY OF TECHNOLOGY